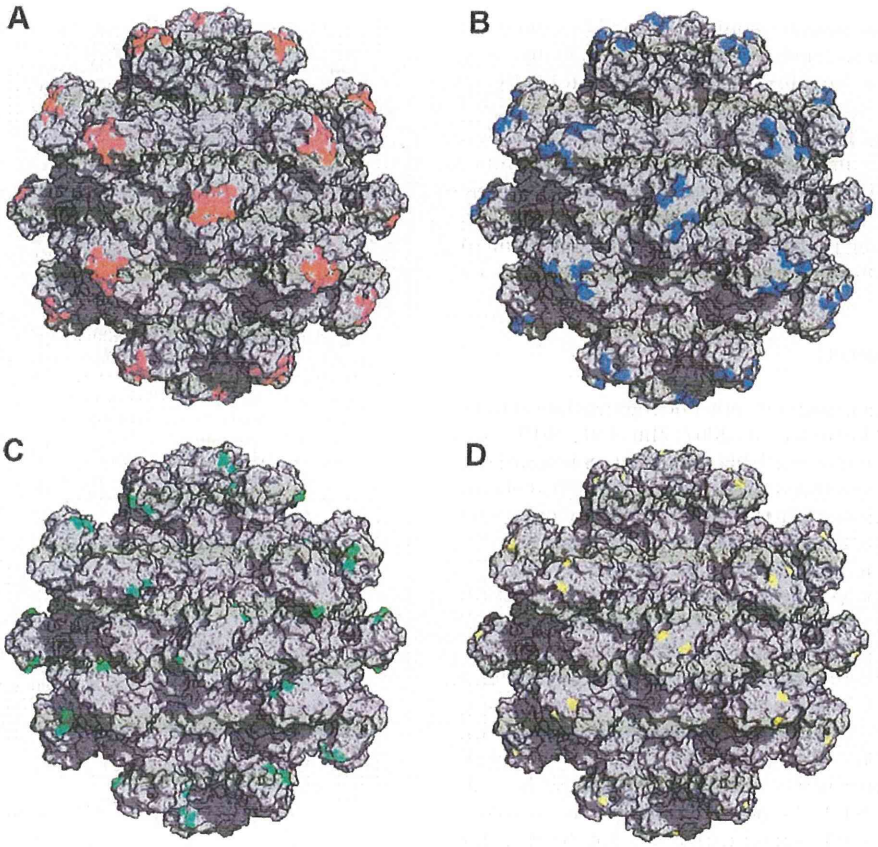

Fig. 4. Functional domains mapped in the surface diagrams of HEV-LP. Amino acid residues involved in the cell-attachment (A; red) and in the recognition by NOB antibodies, MAB1323 (B; blue) and MAB272 (C; green), were determined in the previous study (Yamashita et al., 2009). (D) One of the potential N-glycosylation sites, Asn562 (yellow), was located near the cell-attachment region and the epitope of MAB1323.

Several neutralizing or neutralizing-of-binding (NOB) antibodies against the HEV capsid protein were reported (Emerson et al., 2006; He et al., 2008; Schofield et al., 2000, 2003; Takahashi et al., 2008a; Yamashita et al., 2009). The NOB antibodies inhibit cell-attachment of HEV-LP/$T=1$. The linear epitopes were found in the M and P domains (He et al., 2008; Schofield et al., 2000) while the conformational epitopes were in the P domain (Yamashita et al., 2009), suggesting that the M and P domains play a role on entry steps. Especially, the epitopes of the neutralizing antibody reported by Schofield et al. (2000) and the NOB antibody MAB1323 by us (Yamashita et al., 2009) were mapped at the apical region of the protruding spike, overlapping with the cell-attachment region (Fig. 4B). Thus, these antibodies could physically hamper the attachment of HEV-LP/$T=1$. Another NOB antibody MAB272 in our study recognized the side surface of the P domain just over the M domain (Yamashita et al., 2009) (Fig. 4C). The result might support an involvement of the M domain in entry steps although it is unclear the mechanism. Guu et al. (2009) found the structural similarity of the HEV M domain to the endosialidase of bacteriophage K1F, which binds to sialic acid molecules. Therefore, the M domain might be involved in binding to another cell receptors.

7. Glycosylation of the HEV capsid protein

Because of a lack of the signal peptide-like sequence of the HEV-LP capsid protein, it was not glycosylated in spite of containing the three potential N-glycosylation sites, Asn137, Asn310 and Asn562. In the 3D structure of HEV-LP/$T=1$, Asn137 is mapped adjacent to the interface of the capsid pentamer and Asn310 is completely hidden by the interface of the capsid subunit trimer. Therefore, if it occurs at all, this modification at these sites will interfere the assembly of at least HEV-LP/$T=1$. Interestingly, Asn562 was located in the apical center of the protruding spike as well as the cell-attachment region and antigenic sites of some neutralizing antibodies (Fig. 4D). Sugar chain at Asn562 probably masks these regions. Therefore, it is supposed that non-glycosylated form of the capsid protein assembles into fully functional virus particle while the glycosylated form works unknown functions other than particle assembly.

8. A packaging model of a native $T=3$ virion

Viruses with a $T=3$ symmetry often produces $T=1$ small particles. Both particles are generally composed of identical capsid subunit but of different copy numbers ($T=3$; 180 subunits, $T=1$; 60 subunits). Previous studies on plant tombusviruses indicated that the N-terminal domain played an important role in switching of transition from $T=3$ to $T=1$ symmetry (Hsu et al., 2006; Kakani et al., 2008). In this context, it is thought that HEV-LP/$T=1$ production is caused by deletion of the N-terminal basic domain and the native virion has a $T=3$ symmetry. A recent report by Xing et al. (2010) strongly supported this concept. Upon infection in insect cells with the recombinant baculovirus harboring the HEV capsid protein with deletion of the only N-terminal 13 amino acids, two kinds of particles, HEV-LP/$T=1$ and HEV-LP/$T=3$, which were composed of approximately 53 kDa and 64 kDa capsid proteins, respectively, were yielded. They successfully illustrated cryoelectron microscopy image of HEV-LP/$T=3$. The HEV-LP/$T=3$ had an overall diameter of 410 Å. The HEV-LP/$T=3$ had a $T=3$ symmetry and was composed of 180 copies of the capsid protein, which

Please cite this article in press as: Mori, Y., Matsuura, Y., Structure of hepatitis E viral particle. Virus Res. (2011), doi:10.1016/j.virusres.2011.03.015

were grouped into three unique monomers (A, B and C monomers) according to their geometric environments. Similar to many other $T=3$ viruses, A and B subunits formed the dimer with bent conformation around the 5-fold icosahedral axis, while C monomers formed the dimer with flat conformation at the 2-fold icosahedral axis. Interestingly, the orientation of the P domain of the C–C dimer of HEV-LP/$T=3$ relative to its M and S domains was approximately 90° different to those of the A–B dimer of HEV-LP/$T=3$ and the dimer of HEV-LP/$T=1$. The proline-rich hinge linking the P and M domains was likely to contribute to this transition of the P domain orientation.

9. Conclusion and subjects

HEV capsid polypeptides are currently undergoing clinical trials as vaccine candidates (Shrestha et al., 2007; Zhu et al., 2010). Furthermore, HEV-LP/$T=1$ may be available as a carrier for foreign DNA (Takamura et al., 2004) or epitopes (Niikura et al., 2002). Recent progresses in the structural studies on HEV particles will provide useful information not only for evaluation of HEV life cycles such as assembly, entry to cells and disassembly but also for the development of such monovalent or polyvalent vaccines. However, several subjects still remain in the structural study. First, the structure of the whole capsid protein has not been resolved. Particularly, it is possible that the C-terminal amino acids deleted in the capsid protein of HEV-LPs might integrates folding and functions of the protruding spike. Another subject is that the existences of two types of virions, nonenveloped virions found in fecal samples and "enveloped" virions found in serum samples, were suggested (Takahashi et al., 2008b; Yamada et al., 2009). It was reported that the envelope virus associated with the ORF3 protein and lipids, but the structure is largely unclear. Further studies are required to evaluate these subjects.

Acknowledgements

We thank H. Murase for her secretarial work. This work was supported in part by grants-in-aid from the Research and Development Program for New Bioindustry Initiatives of Bio-oriented Technology Research Advancement Institution (BRAIN) and the Foundation for Research Collaboration Center on Emerging and Re-emerging infections.

References

Balayan, M.S., Andjaparidze, A.G., Savinskaya, S.S., Ketiladze, E.S., Braginsky, D.M., Savinov, A.P., Poleschuk, V.F., 1983. Evidence for a virus in non-A, non-B hepatitis transmitted via the fecal–oral route. Intervirology 20, 23–31.
Bhella, D., Gatherer, D., Chaudhry, Y., Pink, R., Goodfellow, I.G., 2008. Structural insights into calicivirus attachment and uncoating. J. Virol. 82, 8051–8058.
Bradley, D., Andjaparidze, A., Cook Jr., E.H., McCaustland, K., Balayan, M., Stetler, H., Velazquez, O., Robertson, B., Humphrey, C., Kane, M., et al., 1988. Aetiological agent of enterically transmitted non-A, non-B hepatitis. J. Gen. Virol. 69 (Pt 3), 731–738.
Bu, W., Mamedova, A., Tan, M., Xia, M., Jiang, X., Hegde, R.S., 2008. Structural basis for the receptor binding specificity of Norwalk virus. J. Virol. 82, 5340–5347.
Chen, R., Neill, J.D., Estes, M.K., Prasad, B.V., 2006. X-ray structure of a native calicivirus: structural insights into antigenic diversity and host specificity. Proc. Natl. Acad. Sci. U. S. A. 103, 8048–8053.
Choi, J.M., Hutson, A.M., Estes, M.K., Prasad, B.V., 2008. Atomic resolution structural characterization of recognition of histo-blood group antigens by Norwalk virus. Proc. Natl. Acad. Sci. U. S. A. 105, 9175–9180.
Emerson, S.U., Clemente-Casares, P., Moiduddin, N., Arankalle, V.A., Torian, U., Purcell, R.H., 2006. Putative neutralization epitopes and broad cross-genotype neutralization of hepatitis E virus confirmed by a quantitative cell-culture assay. J. Gen. Virol. 87, 697–704.
Guu, T.S., Liu, Z., Ye, Q., Mata, D.A., Li, K., Yin, C., Zhang, J., Tao, Y.J., 2009. Structure of the hepatitis E virus-like particle suggests mechanisms for virus assembly and receptor binding. Proc. Natl. Acad. Sci. U. S. A. 106, 12992–12997.
He, S., Miao, J., Zheng, Z., Wu, T., Xie, M., Tang, M., Zhang, J., Ng, M.H., Xia, N., 2008. Putative receptor-binding sites of hepatitis E virus. J. Gen. Virol. 89, 245–249.
Hsu, C., Singh, P., Ochoa, W., Manayani, D.J., Manchester, M., Schneemann, A., Reddy, V.S., 2006. Characterization of polymorphism displayed by the coat protein mutants of tomato bushy stunt virus. Virology 349, 222–229.
Jameel, S., Zafrullah, M., Ozdener, M.H., Panda, S.K., 1996. Expression in animal cells and characterization of the hepatitis E virus structural proteins. J. Virol. 70, 207–216.
Johne, R., Plenge-Bonig, A., Hess, M., Ulrich, R.G., Reetz, J., Schielke, A., 2010. Detection of a novel hepatitis E-like virus in faeces of wild rats using a nested broad-spectrum RT-PCR. J. Gen. Virol. 91, 750–758.
Kakani, K., Reade, R., Katpally, U., Smith, T., Rochon, D., 2008. Induction of particle polymorphism by cucumber necrosis virus coat protein mutants in vivo. J. Virol. 82, 1547–1557.
Kalia, M., Chandra, V., Rahman, S.A., Sehgal, D., Jameel, S., 2009. Heparan sulfate proteoglycans are required for cellular binding of the hepatitis E virus ORF2 capsid protein and for viral infection. J. Virol. 83, 12714–12724.
Li, S., Tang, X., Seetharaman, J., Yang, C., Gu, Y., Zhang, J., Du, H., Shih, J.W., Hew, C.L., Sivaraman, J., Xia, N., 2009. Dimerization of hepatitis E virus capsid protein E2s domain is essential for virus–host interaction. PLoS Pathog. 5, e1000537.
Li, T.C., Scotti, P.D., Miyamura, T., Takeda, N., 2007. Latent infection of a new alphanodavirus in an insect cell line. J. Virol. 81, 10890–10896.
Li, T.C., Suzaki, Y., Ami, Y., Dhole, T.N., Miyamura, T., Takeda, N., 2004. Protection of cynomolgus monkeys against HEV infection by oral administration of recombinant hepatitis E virus-like particles. Vaccine 22, 370–377.
Li, T.C., Takeda, N., Miyamura, T., Matsuura, Y., Wang, J.C., Engvall, H., Hammar, L., Xing, L., Cheng, R.H., 2005. Essential elements of the capsid protein for self-assembly into empty virus-like particles of hepatitis E virus. J. Virol. 79, 12999–13006.
Li, T.C., Yamakawa, Y., Suzuki, K., Tatsumi, M., Razak, M.A., Uchida, T., Takeda, N., Miyamura, T., 1997. Expression and self-assembly of empty virus-like particles of hepatitis E virus. J. Virol. 71, 7207–7213.
Niikura, M., Takamura, S., Kim, G., Kawai, S., Saijo, M., Morikawa, S., Kurane, I., Li, T.C., Takeda, N., Yasutomi, Y., 2002. Chimeric recombinant hepatitis E virus-like particles as an oral vaccine vehicle presenting foreign epitopes. Virology 293, 273–280.
Okamoto, H., 2007. Genetic variability and evolution of hepatitis E virus. Virus Res. 127, 216–228.
Panda, S.K., Thakral, D., Rehman, S., 2007. Hepatitis E virus. Rev. Med. Virol. 17, 151–180.
Prasad, B.V., Hardy, M.E., Dokland, T., Bella, J., Rossmann, M.G., Estes, M.K., 1999. X-ray crystallographic structure of the Norwalk virus capsid. Science 286, 287–290.
Schofield, D.J., Glamann, J., Emerson, S.U., Purcell, R.H., 2000. Identification by phage display and characterization of two neutralizing chimpanzee monoclonal antibodies to the hepatitis E virus capsid protein. J. Virol. 74, 5548–5555.
Schofield, D.J., Purcell, R.H., Nguyen, H.T., Emerson, S.U., 2003. Monoclonal antibodies that neutralize HEV recognize an antigenic site at the carboxyterminus of an ORF2 protein vaccine. Vaccine 22, 257–267.
Shrestha, M.P., Scott, R.M., Joshi, D.M., Mammen Jr., M.P., Thapa, G.B., Thapa, N., Myint, K.S., Fourneau, M., Kuschner, R.A., Shrestha, S.K., David, M.P., Seriwatana, J., Vaughn, D.W., Safary, A., Endy, T.P., Innis, B.L., 2007. Safety and efficacy of a recombinant hepatitis E vaccine. N. Engl. J. Med. 356, 895–903.
Sreenivasan, M.A., Arankalle, V.A., Sehgal, A., Pavri, K.M., 1984. Non-A, non-B epidemic hepatitis: visualization of virus-like particles in the stool by immune electron microscopy. J. Gen. Virol. 65 (Pt 5), 1005–1007.
Takahashi, M., Hoshino, Y., Tanaka, T., Takahashi, H., Nishizawa, T., Okamoto, H., 2008a. Production of monoclonal antibodies against hepatitis E virus capsid protein and evaluation of their neutralizing activity in a cell culture system. Arch. Virol. 153, 657–666.
Takahashi, M., Yamada, K., Hoshino, Y., Takahashi, H., Ichiyama, K., Tanaka, T., Okamoto, H., 2008b. Monoclonal antibodies raised against the ORF3 protein of hepatitis E virus (HEV) can capture HEV particles in culture supernatant and serum but not those in feces. Arch. Virol. 153, 1703–1713.
Takamura, S., Niikura, M., Li, T.C., Takeda, N., Kusagawa, S., Takebe, Y., Miyamura, T., Yasutomi, Y., 2004. DNA vaccine-encapsulated virus-like particles derived from an orally transmissible virus stimulate mucosal and systemic immune responses by oral administration. Gene Ther. 11, 628–635.
Xing, L., Kato, K., Li, T., Takeda, N., Miyamura, T., Hammar, L., Cheng, R.H., 1999. Recombinant hepatitis E capsid protein self-assembles into a dual-domain $T=1$ particle presenting native virus epitopes. Virology 265, 35–45.
Xing, L., Li, T.C., Miyazaki, N., Simon, M.N., Wall, J.S., Moore, M., Wang, C.Y., Takeda, N., Wakita, T., Miyamura, T., Cheng, R.H., 2010. Structure of hepatitis E virion-sized particle reveals an RNA-dependent viral assembly pathway. J. Biol. Chem..
Yamada, K., Takahashi, M., Hoshino, Y., Takahashi, H., Ichiyama, K., Nagashima, S., Tanaka, T., Okamoto, H., 2009. ORF3 protein of hepatitis E virus is essential for virion release from infected cells. J. Gen. Virol. 90, 1880–1891.
Yamashita, T., Mori, Y., Miyazaki, N., Cheng, R.H., Yoshimura, M., Unno, H., Shima, R., Moriishi, K., Tsukihara, T., Li, T.C., Takeda, N., Miyamura, T., Matsuura, Y., 2009. Biological and immunological characteristics of hepatitis E virus-like particles based on the crystal structure. Proc. Natl. Acad. Sci. U. S. A. 106, 12986–12991.
Zhu, F.C., Zhang, J., Zhang, X.F., Zhou, C., Wang, Z.Z., Huang, S.J., Wang, H., Yang, C.L., Jiang, H.M., Cai, J.P., Wang, Y.J., Ai, X., Hu, Y.M., Tang, Q., Yao, X., Yan, Q., Xian, Y.L., Wu, T., Li, Y.M., Miao, J., Ng, M.H., Shih, J.W., Xia, N.S., 2010. Efficacy and safety of a recombinant hepatitis E vaccine in healthy adults: a large-scale, randomised, double-blind placebo-controlled, phase 3 trial. Lancet 376, 895–902.

Please cite this article in press as: Mori, Y., Matsuura, Y., Structure of hepatitis E viral particle. Virus Res. (2011), doi:10.1016/j.virusres.2011.03.015

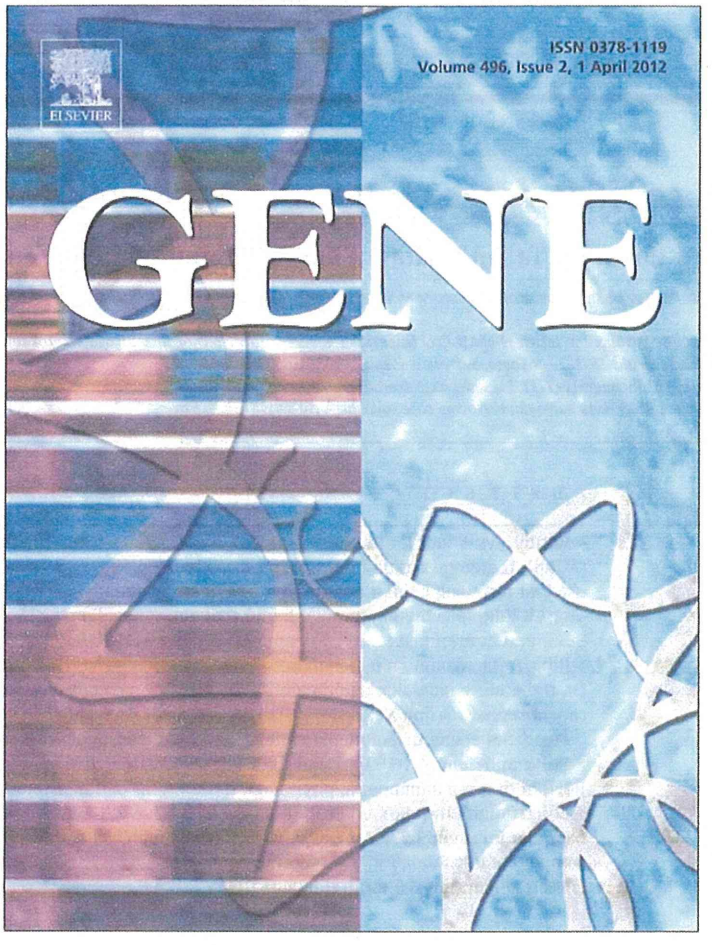

Gene 496 (2012) 79–87

Contents lists available at SciVerse ScienceDirect

Gene

journal homepage: www.elsevier.com/locate/gene

Detergent-induced activation of the hepatitis C virus genotype 1b RNA polymerase

Leiyun Weng [a], Michinori Kohara [b], Takaji Wakita [c], Kunitada Shimotohno [d], Tetsuya Toyoda [a,b,e,*]

[a] Unit of Viral Genome Regulation, Institut Pasteur of Shanghai, Key Laboratory of Molecular Virology & Immunology, Chinese Academy of Sciences, 411 Hefei Road, Shanghai 200025, PR China
[b] Infectious Disease Regulation Project, Tokyo Metropolitan Institute of Medical Sciences, 1-6, Kamikitazawa 2-chome, Setagaya-ku, Tokyo 156-8506, Japan
[c] Department of Virology II, National Institute of Health, 1-23-1 Toyama, Shinjuku, Tokyo 132-8640, Japan
[d] Affiliated Research Institute, Chiba Institute of Technology, 2-17-1 Tsudamuna, Narashino, Chiba 275-0016, Japan
[e] Choju Medical Institute, Fukushimura Hospital, 19-4 Azanakayama, Noyori-cho, Toyohashi, Aichi 441-8124, Japan

ARTICLE INFO

Article history:
Accepted 18 January 2012
Available online 28 January 2012

Keywords:
HCV
NS5B
RNA polymerase
In vitro transcription
Triton X-100
Oligomer

ABSTRACT

Recently, we found that sphingomyelin bound and activated hepatitis C virus (HCV) 1b RNA polymerase (RdRp), thereby recruiting the HCV replication complex into lipid raft structures. Detergents are commonly used for resolving lipids and purifying proteins, including HCV RdRp. Here, we tested the effect of detergents on HCV RdRp activity in vitro and found that non-ionic (Triton X-100, NP-40, Tween 20, Tween 80, and Brij 35) and twitterionic (CHAPS) detergents activated HCV 1b RdRps by 8–16.6 folds, but did not affect 1a or 2a RdRps. The maximum effect of these detergents was observed at around their critical micelle concentrations. On the other hand, ionic detergents (SDS and DOC) completely inactivated polymerase activity at 0.01%. In the presence of Triton X-100, HCV 1b RdRp did not form oligomers, but recruited more template RNA and increased the speed of polymerization. Comparison of polymerase and RNA-binding activity between JFH1 RdRp and Triton X-100-activated 1b RdRp indicated that monomer RdRp showed high activity because JFH1 RdRp was a monomer in physiological conditions of transcription. Besides, 502H plays a key role on oligomerization of 1b RdRp, while 2a RdRps which have the amino acid S at position 502 are monomers. This oligomer formed by 502H was disrupted both by high salt and Triton X-100. On the contrary, HCV 1b RdRp completely lost fidelity in the presence of 0.02% Triton X-100, which suggests that caution should be exercised while using Triton X-100 in anti-HCV RdRp drug screening tests.

1. Introduction

Hepatitis C virus (HCV) belongs to the family *Flaviviridae* and has a positive-stranded RNA genome (Lemon et al., 2007). HCV chronically infects more than 130 million people worldwide (Wasley and Alter, 2000), and infection often induces liver cirrhosis and/or hepatocellular carcinoma (Kiyosawa et al., 1990; Saito et al., 1990). The 9.6-kb-long HCV RNA genome has a long open reading frame encoding a polyprotein of approximately 3,010 amino acids, which is processed into at least 10 viral proteins (NH_2-C-E1-E2-p7-NS2-NS3-NS4A-NS4B-NS5A-NS5B-COOH) by host and viral proteases (Grakoui et al., 1993; Hijikata et al., 1993). The 5′-untranslated region (UTR) contains the internal ribosome entry site (IRES) (Tsukiyama-Kohara et al., 1992). The 3′-UTR contains a poly pyrimidine "U/C" tract, a variable region, and 98-base X-region (Tanaka et al., 1996).

HCV RNA replication depends on the association between the viral protein and raft membranes (Shi et al., 2003; Aizaki et al., 2004), where NS5B RNA polymerase (RdRp) localizes by binding to sphingomyelin (Sakamoto et al., 2005). HCV RdRp is a key enzyme involved in the transcription and replication of the viral genome, and an important target of antivirals. Recently, we found that sphingomyelin bound to and activated HCV 1b RdRp, thereby recruiting the HCV replication complex into lipid raft structures (Weng et al., 2010).

Detergents are commonly used for solubilizing proteins from the lipid-containing components. Some restriction enzymes, reverse transcriptases, and Taq polymerases are stabilized by Triton X-100 or NP-40 (Weyant et al., 1990), while some other polymerases are activated by detergents (Thompson et al., 1972; Wu and Cetta, 1975; Hirschman et al., 1978). Triton X-100 is used for purification of HCV RdRp (Weng et al., 2009). Oligomerization of HCV RdRp is important for its activity (Qin et al., 2002; Clemente-Casares et al., 2011). We have developed an in vitro HCV de novo transcription system by using soluble RdRp and the complementary sequence of the 5′-HCV

Abbreviations: CHAPS, 3-[(3-cholanidopropyl)dimethylammonio]-1-propanesulfonate; CMC, critical micelle concentration; DOC, sodium deoxycholate; HCV, hepatitis C virus; IRES, internal ribosome entry site; KGlu, monopotassium glutamate; PMSF, phenylmethanesulfonyl fluoride; RdRp, RNA polymerase; SDS, sodium dodecyl sulfate; TNTase, terminal nucleotidyl transferase; UTR, untranslated region; nOG, octyl-β-glucoside.

* Corresponding author at: Choju Medical Institute, Fukushimura Hospital, 19-4 Azanakayama, Noyori-cho, Toyohashi, Aichi 441-8124, Japan. Tel.: +81 532 46 7511; fax: +81 532 46 8940.
E-mail address: toyoda_tetsuya@yahoo.co.jp (T. Toyoda).

0378-1119/$ – see front matter © 2012 Elsevier B.V. All rights reserved.
doi:10.1016/j.gene.2012.01.044

genome RNA (SL12-1S template) (Kashiwagi et al., 2002a; Kashiwagi et al., 2002b; Weng et al., 2009; Murayama et al., 2010; Weng et al., 2010). In this paper, we analyzed the effect of detergents on the activity and oligomerization of HCV RdRp, and found that non-ionic (Triton X-100, NP-40, Tween 20, Tween 80, and Brij 35) and twitterionic (3-[(3-cholanidopropyl)dimethylammonio]-1-propanesulfonate [CHAPS]) detergents activated HCV 1b RdRp. In addition, we analyzed the mechanism of RdRp activation by detergents and the relationship between RdRp oligomerization and its activity.

2. Materials and methods

2.1. Mutant HCV RdRp

The H502S mutation of HCR6 (1b) RdRp and the S502H mutation of JFH1 (2a) were introduced using an in vitro mutagenesis kit (Stratagene). Oligonucleotide sequence information is available upon request.

2.2. Purification of HCV RdRp from bacteria

HCV HCR6wt (1b) (Weng et al., 2009), NN (1b) (Watashi et al., 2005), Con1 (1b) (Binder et al., 2007), JFH1wt (2a) (Weng et al., 2009), J6CF (2a) (Murayama et al., 2007), H77 (1a) (Blight et al., 2003), RMT (1a), HCR6 (1b) H502S, and JFH1 (2a) H502S RdRps with a C-terminal 21-amino acid deletion were purified from bacteria as previously described with some modifications (Weng et al., 2009, 2010; Murayama et al., 2010). Briefly, HCV RdRps were eluted from Ni-NTA agarose (Qiagen) with 20 mM Tris–HCl (pH 8.0), 500 mM NaCl, 0.1% Triton X-100, 0.1% 2-mercaptoethanol, and 1 mM phenylmethanesulfonyl fluoride (PMSF) containing 250 mM imidazole after the column was washed with 5 mM imidazole. HCV RdRps were further purified through a Superdex 200 pg column (GE Healthcare) in 20 mM Tris–HCl (pH 8.0), 500 mM NaCl, 1 mM EDTA, 5 mM DTT, 10% glycerol, and 1 mM PMSF to remove contaminating nucleic acids (Fig. S1). The purified HCV RdRps were stored at −80 °C.

2.3. De novo HCV RdRp assay

HCV RdRp assay in the absence of primers was performed as described previously (Weng et al., 2009; Murayama et al., 2010). Briefly, following a 30-min pre-incubation period without ATP, CTP, or UTP, 100 nM HCV RdRp were incubated in 50 mM Tris–HCl (pH 8.0), 200 mM monopotassium glutamate (KGlu), 3.5 mM $MnCl_2$, 1 mM DTT, 0.5 mM GTP, 50 μM ATP, 50 μM CTP, 5 μM [α-^{32}P]UTP, 200 nM 184-nt model RNA template (SL12-1S) (Kashiwagi et al., 2002a; Weng et al., 2009; Murayama et al., 2010), 100 U/ml human placental RNase inhibitor, and the indicated amount of detergent at 29 °C for 90 min. [^{32}P]RNA products were separated in a 6% polyacrylamide gel containing 8 M urea. The resulting autoradiograph was analyzed with a Typhoon Trio Plus image analyzer (GE Healthcare) for the radio activity of 184-nt transcription products.

2.4. Kinetic analysis of HCV RdRp with and without Triton X-100

Kinetic analysis (measurement of *Km* and *Vmax*) was performed as previously published with and without 0.02% Triton X-100 (Kashiwagi et al., 2002b; Weng et al., 2009). For *Km* and *Vmax* of ATP, HCV RdRp was incubated in 50, 25, 10, 8, 5, 3, or 1 μM of ATP, 50 μM CTP, 0.5 mM GTP, 5 μM [α-^{32}P]UTP after preincubation in 0.5 mM GTP with and without 0.02% Triton X-100 at 29 °C for 60 min. For *Km* and *Vmax* of CTP, 50, 25, 10, 8, 5, 3, or 1 μM of CTP, 50 μM ATP, 0.5 mM GTP, and 5 μM [α-^{32}P]UTP, and for *Km* and *Vmax* of UTP, 50, 25, 10, 8, 5, 3, or 1 μM of UTP, 50 μM ATP, 0.5 mM GTP, 5 μM [α-^{32}P]CTP were used, respectively. For *Km* and *Vmax* of GTP, HCV RdRp was incubated in 500, 250, 100, 50, 25, 10, or 5 μM of GTP, 50 μM ATP, 50 μM CTP, 5 μM [α-^{32}P]UTP with and without 0.02% Triton X-100 without GTP preincubation.

2.5. Terminal nucleotidyl transferase (TNTase) assay

TNTase assay was performed with the heat denatured 5′-[^{32}P] sym/sub (5′-GAUCGGGCCCGAUC-3′) (Arnold and Cameron, 2000) with 0.5 mM GTP, 50 μM ATP, 50 μM CTP, and 50 μM UTP, and sym/sub with 0.5 mM GTP, 50 μM ATP, 50 μM CTP, and 5 μM [α-^{32}P]-UTP in the same experimental conditions as the above-described transcription assay (Hong et al., 2001). [^{32}P]RNA products were separated in a 15% polyacrylamide gel containing 8 M urea.

2.6. RNA filter-binding assay

RNA filter-binding assays were performed as previously described (Weng et al., 2009). Briefly, 100 nM of HCV RdRp and 100 nM [^{32}P] RNA template (SL12-1S) were incubated with the indicated amount of detergent in 25 μl of 50 mM Tris–HCl (pH 7.5), 200 mM KGlu, 3.5 mM $MnCl_2$, and 1 mM DTT at 29 °C for 30 min. After incubation, the solutions were diluted with 0.5 ml TE and filtered through nitrocellulose membranes (0.45 μm; Millipore). The filter was washed 5 times with TE, and the bound radioisotope was analyzed using the Typhoon Trio Plus image analyzer after being dried.

2.7. Western blot

Western blot analysis using a rabbit anti-HCV RdRp antibody was performed, as described previously (Kashiwagi et al., 2002b).

2.8. Gel filtration

The purified HCR6 (1b), J6CF (2a), and JFH1 (2a) RdRps (50 pmol) were applied on a Superdex 200 pg column in 50 mM Tris–HCl (pH 7.5), 200 mM KGlu or 150 mM NaCl, 3.5 mM $MnCl_2$, 1 mM DTT, and 0.2% glycerol with or without 0.1% Triton X-100.

2.9. Reagents

PMSF, Triton X-100, Tween 20, Tween 80, NP-40, Brij 35, octyl-β-glucoside (nOG), CHAPS, sodium deoxycholate (DOC), and sodium dodecyl sulfate (SDS) were obtained from Amresco; nucleotides were purchased from GE Healthcare; [α-^{32}P]UTP, [α-^{32}P]ATP, [α-^{32}P]GTP, [α-^{32}P]CTP, and [γ-^{32}P]ATP were from New England Nuclear.

2.10. Statistical analysis

Significant differences were determined using the Student's *t*-test.

3. Results

3.1. Effect of detergents on primer-independent HCV RdRp activity

First, we examined the effect of detergents on the primer-independent HCV RdRp activity in vitro (Fig. 1). HCR6 (1b) RdRpwt was activated by all the detergents tests, except octyl-β-glucoside (nOG), but JFH1 (2a) RdRpwt was not. The activation curves of HCR6 (1b) RdRpwt by these detergents plateaued at certain concentrations: 0.002 or 0.004% Triton X-100, 0.001% NP-40, 0.005% Tween 20, 0.001% Tween 80, 0.001% Brij 35, and 0.1% CHAPS. HCR6 (1b) RdRp activity decreased at concentrations greater than 1% Triton X-100, and 30% Triton X-100 completely inhibited HCR6 (1b) RdRpwt activity (Fig. 1A, right panel). With an activation ratio of about 2 at 0.1%, nOG weakly activated HCR6 (1b) RdRpwt. At 0.5% nOG, the

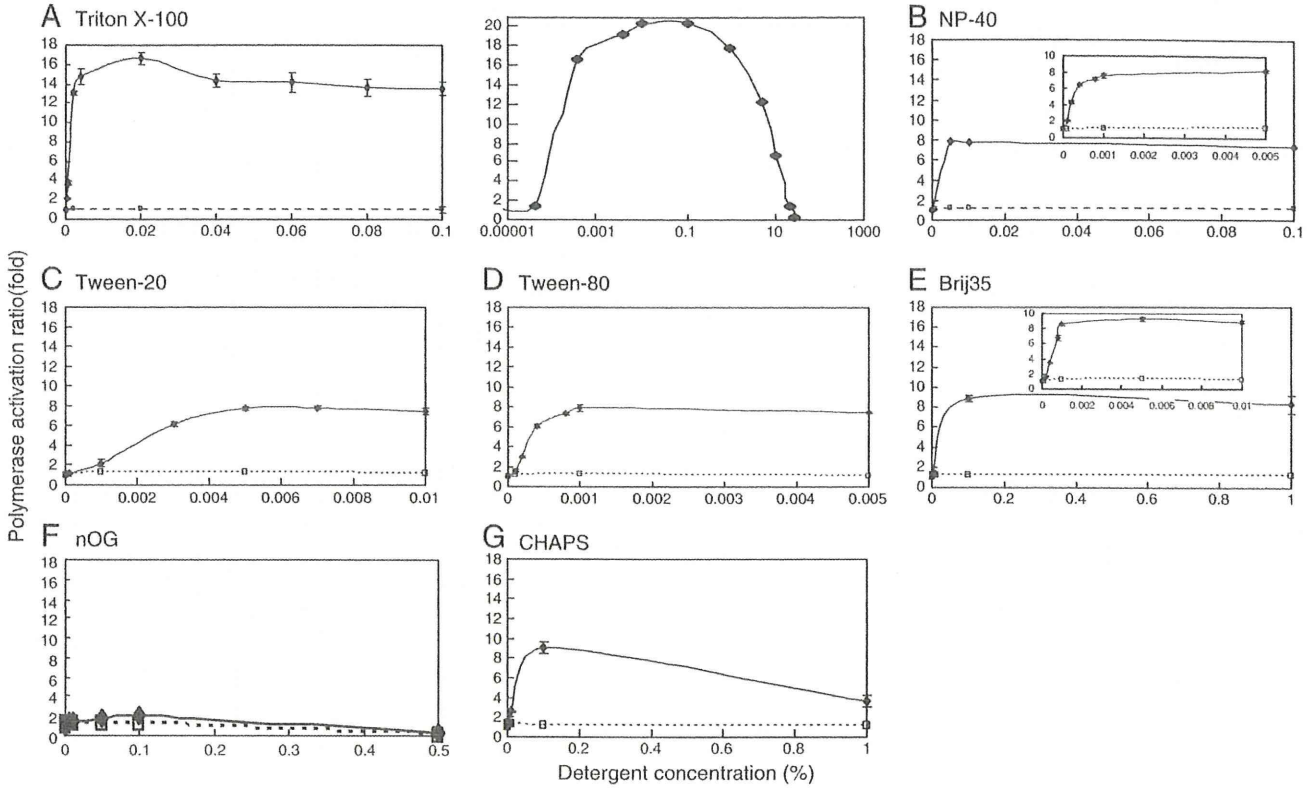

Fig. 1. The effect of detergents on HCV HCR6 and JFH1 RNA polymerases. Wild-type HCR6 (1b) and JFH1 (2a) RdRps were assayed with 0.000004, 0.00004, 0.0004, 0.004, 0.01, 0.02, 0.04, 0.06, 0.08, and 0.1% Triton X-100 (A, left panel); 0.0001, 0.0002, 0.0004, 0.0008, 0.001, 0.005, 0.1, and 0.5% NP-40 (B); 0.0001, 0.001, 0.003, 0.005, 0.007, and 0.01% Tween 20 (C); 0.0001, 0.0002, 0.0004, 0.0008, 0.001, and 0.005% Tween 80 (D); 0.0001, 0.0002, 0.0004, 0.0008, 0.001, 0.005, 0.01, 0.1, and 1% Brij 35 (E); 0.001, 0.005, 0.01, 0.05, and 0.1% nOG (F); or 0.0001, 0.001, 0.005, 0.01, 0.1, 0.1, and 1% CHAPS (G). The effect of high concentration of Triton X-100 on HCR6 (1b) RdRpwt is shown in A (right panel). Inset: Polymerase activation ratio at a lower concentration of NP-40 (B), and Brij 35 (E). Mean and standard deviation (error bar) of the polymerase activation ratio were calculated from 3 independent experiments. The solid line indicates the activation ratio of HCR6 (1b) RdRpwt, and the broken line indicates that of JFH1 (2a) RdRpwt.

activation ratio of HCR6 (1b) RdRpwt was 0.3. At 1% of CHAPS, the activity of HCR6 (1b) RdRpwt was increased by 3.6 folds. The detergent concentration that most activated HCR6 (1b) RdRpwt was approximate to the critical micelle concentration (CMC; Table 1).

When the activation ratios of detergents on HCR6 (1b) RdRpwt were compared, that of Triton X-100 was the highest (Fig. 2, Table 1). Other non-ionic detergents and CHAPS activated HCR6 (1b) RdRpwt to an extent equal to about half of Triton X-100 activation. Although a non-ionic detergent, nOG barely activated HCR6 (1b) RdRpwt.

Because 0.02% Triton X-100 maximally activated HCR6 (1b) RdRpwt, we compared its activation effect on other HCV RdRps (Fig. 3, Table 2). JFH1 (2a) RdRpwt showed the strongest RdRp activity, which is in accordance with previous reports (Weng et al., 2009; Murayama et al., 2010; Schmitt et al., 2011). The RdRp activities of 1b HCR6 and NN activated by Triton X-100 were similar to that of JFH1 RdRpwt in the absence of detergents (Fig. 3B), whereas the RdRp activity of Triton X-100-activated 1b Con1 was about half of that of wild-type JFH1. Neither 1a nor 2a RdRps were activated by Triton X-100.

Table 1
CMC and HCV HCR6 (1b) RdRpwt activation ratio of different detergents.

Detergent	CMC[a] in H_2O (%)	Minimal concentration of maximal activation (%)	Maximal activation (folds)[b]
Triton X-100	0.0155	0.02	16.6 ± 0.56
NP-40	0.0179	0.005	8.3 ± 0.18
Tween 20	0.0074	0.007	7.8 ± 0.21
Tween 80	0.0016	0.001	8.0 ± 0.22
Brij 35	0.1103	0.1	9.2 ± 0.34
nOG	0.672–0.730	0.1	2.1 ± 0.35
CHAPS	0.492–0.615	0.1	9.1 ± 0.60

[a] Modified from "TECHNICAL RESOURCE" (Pierce).
[b] Calculated from Fig. 2.

3.2. RNA template binding with Triton X-100

Next, we compared the template RNA-binding activity of 1a, 1b, and 2a RdRps in the presence of Triton X-100 by using the [^{32}P] SL12-1S model RNA template (Kashiwagi et al., 2002a; Weng et al., 2009, 2010; Murayama et al., 2010) in order to examine the transcription steps activated by Triton X-100 (Fig. 4, Table 2). Template RNA binding was the first step of transcription. The RNA-binding activity of JFH1 RdRpwt was the highest without Triton X-100 (data not shown) (Weng et al., 2009). Different from RdRp activity, the RNA-binding activity of all HCV RdRps was somehow activated by 0.02% Triton X-100. The RNA-binding activity of 1b RdRps was increased by 7–10 folds with Triton X-100.

3.3. Gel filtration of 1b and 2a RdRps

Proteins are generally soluble in detergents. Because HCR6 (1b) RdRpwt showed similar polymerase activity with Triton X-100 as JFH1 (2a) RdRpwt without Triton X-100, we compared the oligomerization state of these RdRps. The oligomerization state of HCR6 (1b) and JFH1 (2a) RdRps under transcription (physiological) conditions (200 mM KGlu or 150 mM NaCl) was analyzed by gel filtration on

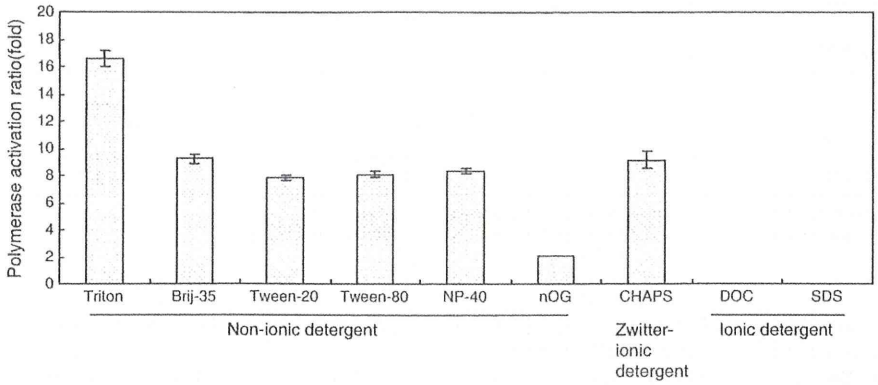

Fig. 2. Activation effect of HCV HCR6 polymerase with detergents at CMC. HCV HCR6 (1b) RdRpwt was assayed at CMC in the presence of Triton X-100 (0.02%), Brij 35 (0.1%), Tween 20 (0.007%), Tween 80 (0.001%), NP40 (0.005%), nOG (0.1%), CHAPS (0.1%), DOC (0.001%), and SDS (0.001%). The activation ratio (fold) is indicated in Table 2. Mean and standard deviation (error bar) of the polymerase activity relative to that without detergent were calculated from 3 independent experiments.

Superdex 200 (Figs. 5 and 6). HCR6 (1b) RdRpwt was eluted from the void volume fraction to the 158-kDa fraction without Triton X-100 (Fig. 5A), which meant that HCR6 (1b) RdRpwt formed random oligomers. It was eluted in the 38-kDa fraction with 0.1% Triton X-100 (Fig. 5B), which indicated that it was smaller than its monomer gel filtration size (Fig. S1D). However, JFH1 (2a) RdRpwt was eluted in the slightly larger fraction (80 kDa) than other HCV RdRps with or without Triton X-100, which indicated the monomer size (Figs. 5C and D, S1F). From the gel filtration and transcription data of HCR6 (1b) RdRpwt and JFH1 (2a) RdRpwt, it was concluded that Triton X-100 dispersed HCR6 (1b) RdRpwt, and that the higher-ordered oligomers of HCR6 (1b) RdRpwt were inactive. Triton X-100 might also affect the interaction between HCR6 (1b) RdRpwt and Superdex200 gel matrix because it was eluted in the smaller molecular weight fractions with Triton X-100 than the monomer gel-filtration size in 0.5 M NaCl (76 kDa, Fig. S1D). Western blot analysis indicated that these RdRp were not degraded (Figs. 5A and B, inset).

Qin et al. found that amino acids 18E and 502H interacted with each other to form the HCV 1b RdRp oligomer/dimer (Qin et al., 2002). Only 2a RdRps harbor the amino acid S at position 502, contrary to other genotype forms of RdRps, which harbor the amino acid H at that same position (Table S1). Therefore, we first examined

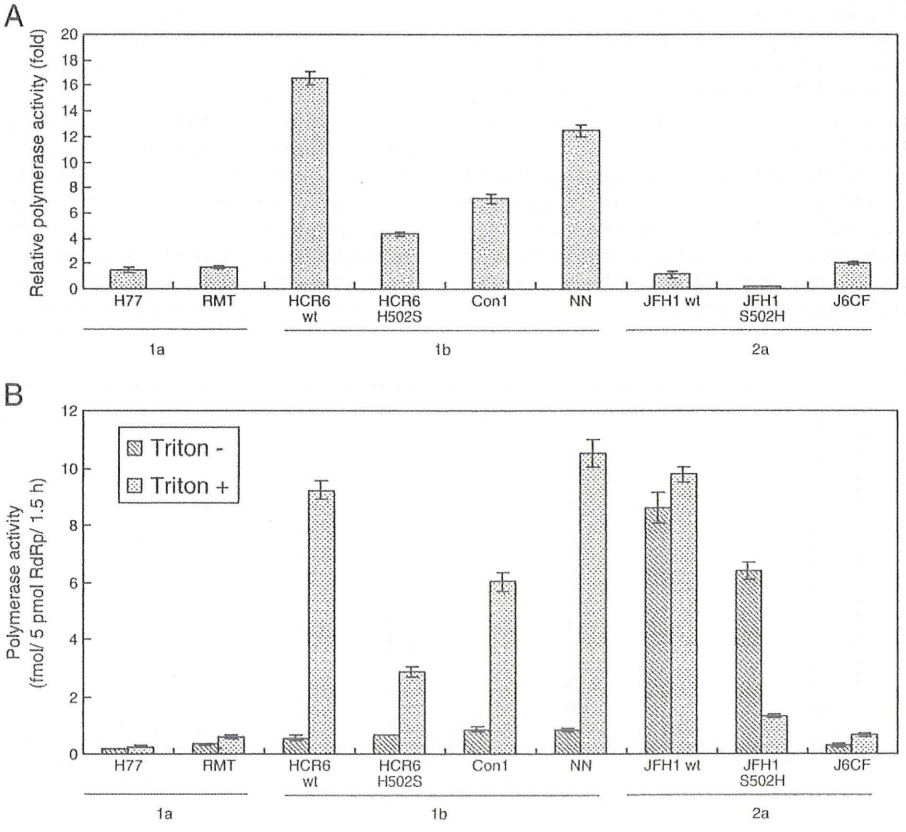

Fig. 3. Effect of 0.02% Triton X-100 on various HCV RNA polymerases. HCV H77 (1a), RMT (1a), HCR6 (1b) wt and H502S, NN (1b), Con1 (1b), JFH1 (2a) wt and S502H, and J6CF (2a) RdRps were assayed in the presence or absence of Triton X-100. A: Activation ratio (fold) of RNA polymerase activity. B: Polymerase activity (fmol of NMP/5 pmol RdRp/1.5 h) in the presence or absence of Triton X-100. Mean and standard deviation (error bar) of the polymerase activity were calculated from 3 independent experiments.

Table 2
Relative activation ratio of HCV RdRp by Triton X-100.

Genotype	1a		1b			2a	
Name	H77	RMT	HCR6	Con1	NN	JFH1	J6CF
Polymerase activity (folds)[a]	1.5 ± 0.17	1.7 ± 0.11	16.6 ± 0.56	7.1 ± 0.38	12.5 ± 0.48	1.1 ± 0.28	2.0 ± 0.12
RNA template-binding activity (folds)[b]	3.8 ± 0.11	3.9 ± 0.18	9.6 ± 0.39	7.9 ± 0.41	6.9 ± 0.16	2.2 ± 0.14	3.4 ± 0.21

[a] Activation ratio of polymerase activity was calculated on the basis of the data represented in Fig. 3A.
[b] Activation ratio of RNA template-binding activity was calculated on the basis of the data represented in Fig. 4A.

another 2a RdRp, J6CF (2a) RdRp, by gel filtration (Fig. 5E). J6CF (2a) RdRp was also eluted as a monomer in 150 mM NaCl buffer without Triton X-100. These gel filtration data was in agreement with the intermolecular interaction and random oligomerization of HCV RdRp caused by 18E and 502E (Qin et al., 2002). Amino acid 18E is shared by HCV RdRps of all 6 genotypes (Table S1) (Clemente-Casares et al., 2011). Therefore, in order to confirm the importance of 502H for oligomerization of HCV RdRp, S502H and H502S mutations were introduced into JFH1 (2a) and HCR6 (1b) RdRps, respectively, and analyzed by gel filtration (Fig. 6). JFH1 (2a) RdRpS502H formed oligomers, and HCR6 (1b) RdRpH502S was eluted in the 15-kDa fraction, which was smaller than its monomeric gel-filtration size. JFH1 (2a) RdRpS502H was eluted around the 50-kDa position with Triton X-100. The RdRp dimers (Qin et al., 2002) were not found in any of our gel filtration profiles. Western blot analysis indicated that the proteins were not degraded (Fig. 6, inset).

The effect of these mutations in RdRp and RNA template-binding activity with and without Triton X-100 was examined (Figs. 3 and 4). JFH1 (2a) RdRpS502H RdRp activity was lower than that of the wild-type in the absence of Triton X-100. Different from the Triton X-100 activation effect on HCR6 (1b) RdRpwt, JFH1 (2a) RdRpS502H RdRp activity decreased, while its RNA template binding increased, in the presence of Triton X-100. HCR6 (1b) RdRpH502S RdRp activity was similar to that of the wild-type, but less activated by Triton X-100 than by the wild-type. RNA template-binding activity of HCR6 (1b) RdRpH502S was activated 2.3 times by Triton X-100.

The 502 mutation data indicated that 502H is important for oligomerization of 1b RdRp molecules in the transcription (physiological salt) condition. Triton X-100 prevented the oligomerization of 1b RdRps by 502H. Moreover, For HCR6 (1b) RdRpwt, the 38-kDa gel filtration molecules (Fig. 5B), which might correspond to the monomer, were more active than the oligomer molecules.

3.4. Fidelity of HCV RdRp with Triton X-100

Finally, we aimed to calculate the kinetic constants (*K*m and *V*max) of HCR6 (1b) RdRp in the presence of 0.02% Triton X-100 because the activation ratio of the polymerase activity was higher than that of RNA binding of HCR6 (1b) RdRp. When nucleotide concentration was low, the amount of product without Triton X-100 decreased; this data can be used to draw Lineweaver–Burk plot (Weng et al., 2009). However, with Triton X-100, the product amount did not decrease according to the decrease of each nucleotide (Fig. 7A). Moreover, each of the nucleotide substrates was removed from the standard HCV in vitro transcription condition (Fig. 7B). Although ATP, CTP or UTP were removed from the reaction buffer, HCV HCR6 (1b) RdRp transcribed the same 184-nt products with Triton X-100, which disappeared without Triton X-100. When GTP was removed, no products were observed with or without Triton X-100 because HCV RdRp required GTP for its structure (Bressanelli et al., 2002). These kinetic experiments indicated that HCV HCR6 (1b) RdRp completely lost fidelity with Triton X-100.

Terminal nucleotidyl transferase (TNTase) activity has been sometimes detected in HCV 1b RdRp preparations (Behrens et al., 1996; Ranjith-Kumar et al., 2001; Ranjith-Kumar et al., 2004; Vo et al., 2004). TNTase activity was not detected in our system, in which the model RNA template contains a CCC-3′ at the 3′-end (Kashiwagi et al., 2002b; Weng et al., 2009). Nevertheless, we examined whether TNTase activity was detected with Triton X-100 using sym/sub, which has GpG-primed transcription activity, but we failed to observe any de novo initiation activity (Hong et al., 2001). No mobility shift was shown by 5′-[^{32}P]sym/sub or sym/sub incubated with [^{32}P]UTP on polyacrylamide gel electrophoresis (PAGE) (Figs. 7C and D), indicating that no TNTase activity was detected in our system with or without Triton X-100.

Apparent *K*m and *V*max of HCR6 (1b) RdRp with Triton X-100 for GTP was 303 ± 15.1 μM and 6.21 ± 0.225/min, respectively (Fig. S3).

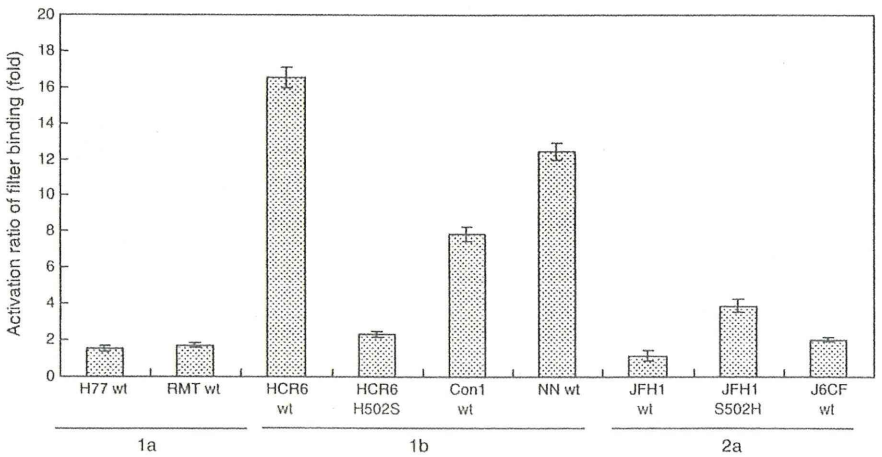

Fig. 4. Effect of 0.02% Triton X-100 on the RNA template-binding activity of HCV RNA polymerases. One hundred nanomolars each of HCV H77 (1a), RMT (1a), HCR6 (1b), NN (1b), Con1 (1b), JFH1 (2a), and J6CF (2a) RdRps with [^{32}P]RNA templates (SL12-1S) were filtered through nitrocellulose membranes after incubation with or without Triton X-100. Mean and standard deviation (error bar) of the RNA filter binding activation (folds) were calculated from 3 independent experiments.

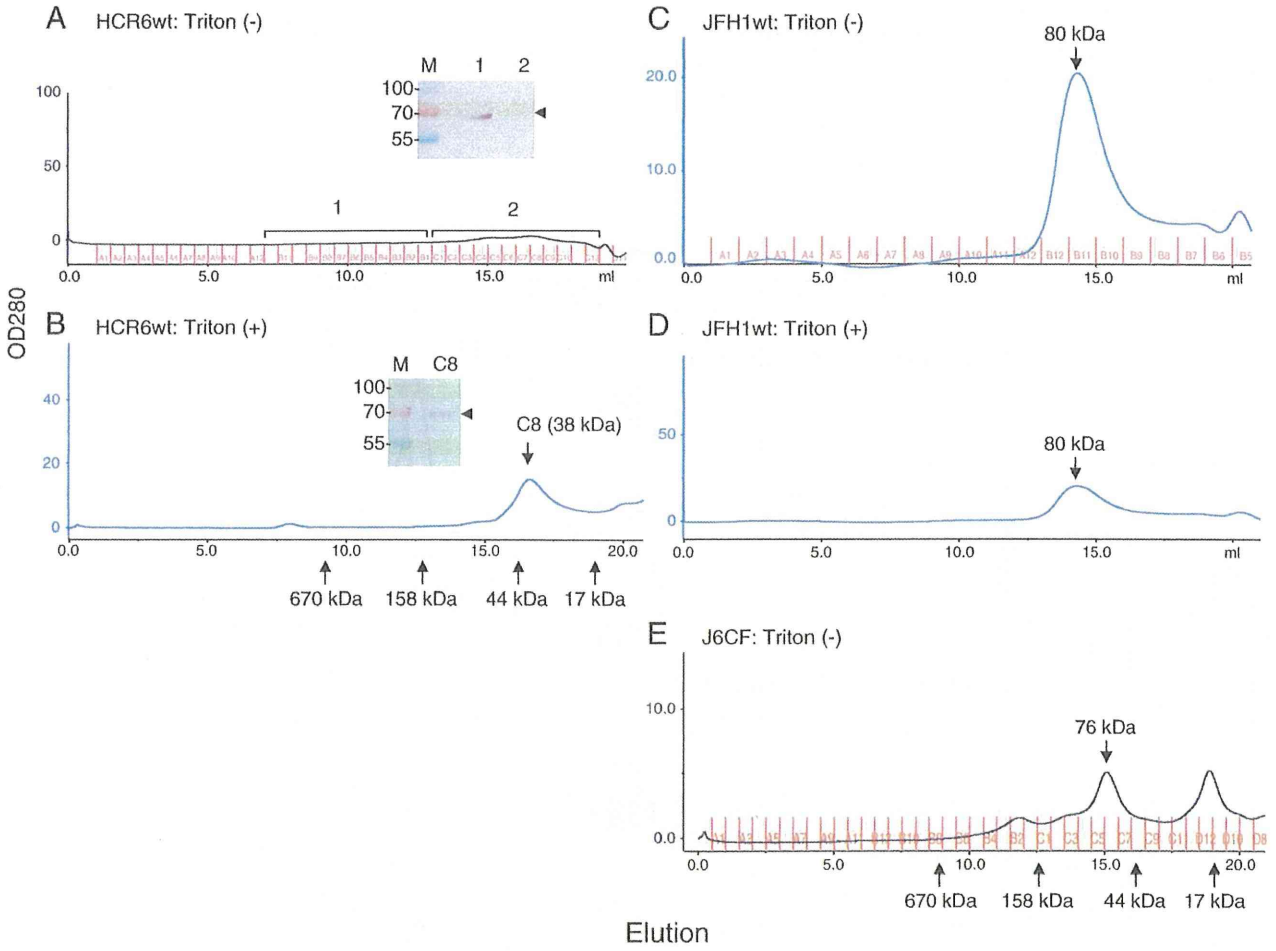

Fig. 5. Superdex 200 gel filtration of HCV HCR6 (1b), JFH1 (2a), and J6CF (2a) wild-type RNA polymerase with or without 0.1% Triton X-100. HCV HCR6 (1b) RdRpwt was applied on Superdex 200 gel filtration columns in 50 mM Tris–HCl (pH 7.5), 150 mM NaCl, 3.5 mM $MnCl_2$, 1 mM DTT, and 0.2% glycerol without (A) or with 0.1% Triton X-100 (B). HCV JFH1 (2a) RdRpwt was applied without (C) or with 0.1% Triton X-100 (D), and J6CF (2a) RdRp was applied without Triton X-100 (E) on the same columns. The elution position of the standard molecular weight markers is indicated below the graph. The molecular weight of the peak fraction is indicated in each graph. Inset in A: The fractions of the void volume–158 kDa (1) and those of lower molecular weight fractions (2) of HCR6 (1b) RdRpwt gel filtration without Triton X-100 were precipitated with TCA and analyzed by western blot. Inset in B: Fraction C8 of HCR6 (1b) RdRpwt with Triton X-100 was precipitated with TCA and analyzed by western blot. The position of HCR6 (1b) RdRpwt is indicated by an arrowhead. The position of the pre-stained size marker is indicated on the left side of the blots.

Km and *Vmax* of HCR6 (1b) RdRp without Triton X-100 for GTP was calculated as 54.7 ± 3.67 μM and 2.52 ± 0.108/min, respectively (Weng et al., 2009).

4. Discussion

Non-ionic (Triton X-100, NP-40, Tween 20, Tween 80, and Brij 35) and twitterionic (CHAPS) detergents activated HCV 1b RdRp by 7.2–16.6 folds when used at their CMC, but did not affect 1a or 2a RdRps (Figs. 1–3, Table 2). In turn, ionic detergents (SDS and DOC) completely inactivated polymerase activity at 0.01%. CMC is the minimum concentration at which a detergent forms micelles; above that concentration, a detergent exists as a large molecular weight complex. The CMC signifies the strength at which a detergent binds to proteins, i.e., low values indicate strong binding, whereas high values indicate weak binding. It is also an indication of the hydrophilicity of a detergent. Triton X-100, NP-40, and Brij 35 at CMC activated Moloney leukemia virus reverse transcriptase by interacting with the hydrophobic domain (Thompson et al., 1972). The activation mechanism of HCV RdRp by these detergents may be similar. However, the detergent interaction domain of HCV RdRp remains to be identified.

Triton X-100 is commonly used for purification of HCV RdRp from the bacteria and insect cells expressing this protein (Lohmann et al., 1997; Luo et al., 2000; Cramer et al., 2006; Weng et al., 2009). HCV 1b RdRp without the C-terminal hydrophobic region expressed in bacteria formed a large molecule complex in 0.1% Triton X-100 or 0,5% CHAPS with a low-salt buffer (<50 mM NaCl) (Qin et al., 2002; Wang et al., 2002). Under low-salt conditions, HCV RdRp was gel filtrated in void volume as a complex with contaminating nucleic acids, because HCV RdRp binds to RNA during purification without high-salt (0.5 M NaCl) stripping (Figs. S1 and S2). Therefore, the presence of HCV 1b RdRp in the void volume fraction of gel filtration by Wang et al. (Wang et al., 2002) could rather represent the complex of HCV RdRp with contaminating nucleic acids. Nevertheless, they also found monomers of HCV 1b RdRp in the gel filtration buffer containing 0.5% CHAPS, which activated polymerase activity (Fig. 1G). Detection of the monomeric HCV 1b RdRps by gel filtration in a buffer containing Triton X-100 and CHAPS has also been reported by other groups (Qin et al., 2002; Wang et al., 2002). HCR6 (1b) RdRpwt formed oligomers in physiological conditions without Triton X-100. In the presence of Triton X-100, HCR6 (1b) RdRpwt was eluted as the monomer which gel-filtration size was smaller than its size in 0.5 M NaCl (Fig. S1D) or calculated from its amino acid composition (64 kDa). HCV 2a (JFH1 and J6CF) RdRps formed a monomer in the same buffer without Triton X-100. Gel filtration analysis of 502 mutants of JFH1 (2a) and HCR6 (1b) RdRps have confirmed that 502H

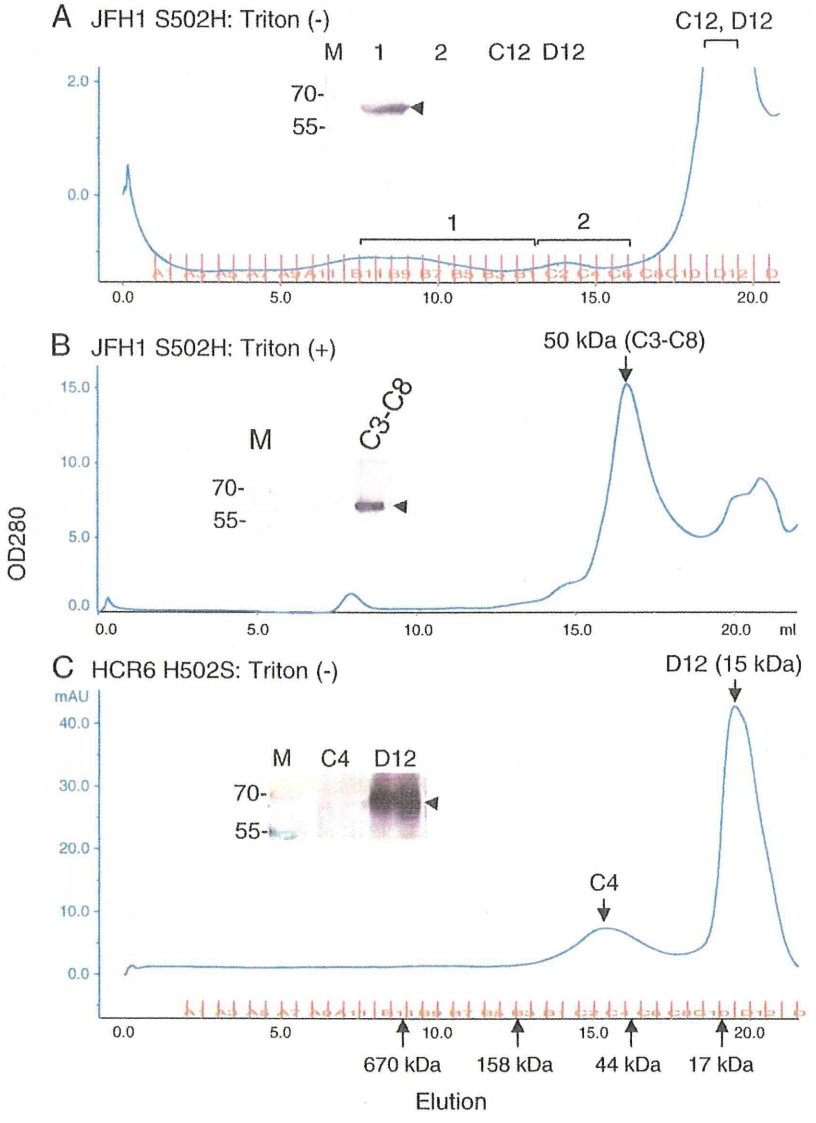

Fig. 6. Superdex 200 gel filtration of HCV JFH1 (2a) and HCR6 (1b) 502 mutant RNA polymerases. JFH1 (2a) S502H (A), and HCR6 (1b) H502S RdRps (C) were applied on Superdex 200 gel filtration columns in 50 mM Tris–HCl (pH 7.5), 150 mM NaCl, 3.5 mM $MnCl_2$, 1 mM DTT, and 0.2% glycerol. JFH1 (2a) RdRpS502H was also applied with 0.1% Triton X-100 (B). Inset in A: The fractions of the void volume—158 kDa (1), those of lower molecular weight fractions (2), fractions C12, and D12 of JFH1 (2a) RdRpS502H gel filtrations were precipitated with TCA and analyzed by western blot. Inset in B: Fraction C3–C8 of JFH1 (2a) RdRpS502H in Triton X-100 were precipitated with TCA and analyzed by western blot. Inset in C: Fractions C4 and D12 of HCR6 (1b) RdRpH502S were precipitated with TCA and analyzed by western blot. The position of HCV RdRp is indicated by an arrowhead. The position of the pre-stained size marker is indicated on the left side of the blots.

is important for the intermolecular interaction of HCV 1b RdRp (Qin et al., 2002). HCV RdRps without the C-terminal hydrophobic domain were soluble in high-salt buffer (>300 mM NaCl; Fig. S1) (Ferrari et al., 1999). The shift to the delayed elution of gel-filtration of HCR6 (1b) RdRpwt and JFH1 (2a) RdRp S502H with Triton X-100, and HCR6 (1b) RdRpH502S may come from the interaction of the RdRps with Superdex200 gel matrix induced by the mutations and Triton X-100.

Our data of HCV RdRp oligomerization at 502H (Fig. 6) are in agreement with those by Qin et al. (Qin et al., 2002), but are contradictory to those obtained by more sensitive methods (fluorescence resonance energy transfer [FRET] and yeast two-hybrid system) (Wang et al., 2002; Clemente-Casares et al., 2011). Interactions between a charged amino acid (His) and an aromatic residue (Trp) (Fernandez-Recio et al., 1997; Matthews et al., 1997; Takeuchi et al., 2003), or His–Glu interactions (Marti and Bosshard, 2003), are often found in proteins. JFH1 (2a) RdRpwt did not form dimers (Chinnaswamy et al., 2010). 502H may interact with 125 W in αF (Clemente-Casares et al., 2011), but not with 18E (Qin et al., 2002). This interaction is dissociated both with high-salt (Fig. S1) and with Triton X-100 (Figs. 5 and 6). Taken together, 502H of HCV 1b RdRp is important for oligomer formation in transcription (physiological salt) conditions. Besides the oligomerization using 502H, the αF and αT helixes of HCV RdRp, which were proposed to be involved in oligomerization (Clemente-Casares et al., 2011), may also be involved in oligomerization of the molecules in transcription condition. The 502 mutations in HCR6 (1b) and JFH1 (2a) RdRps are likely to affect the structure of the template channel by affecting the helix structures of the thumb domain (Bressanelli et al., 2002; Chinnaswamy et al., 2008) because the polymerase and RNA template binding activity of these mutant RdRps was not activated by Triton X-100 (Figs. 3 and 4). These findings indicate the importance around amino acid 502H for HCV 1b RdRp structure. However, these data contradict to the previous reports (Qin et al., 2002; Clemente-Casares et al., 2011).

Comparing the polymerase and template RNA-binding activity of JFH1 (2a) and HCR6 (1b) RdRps with and without Triton X-100,

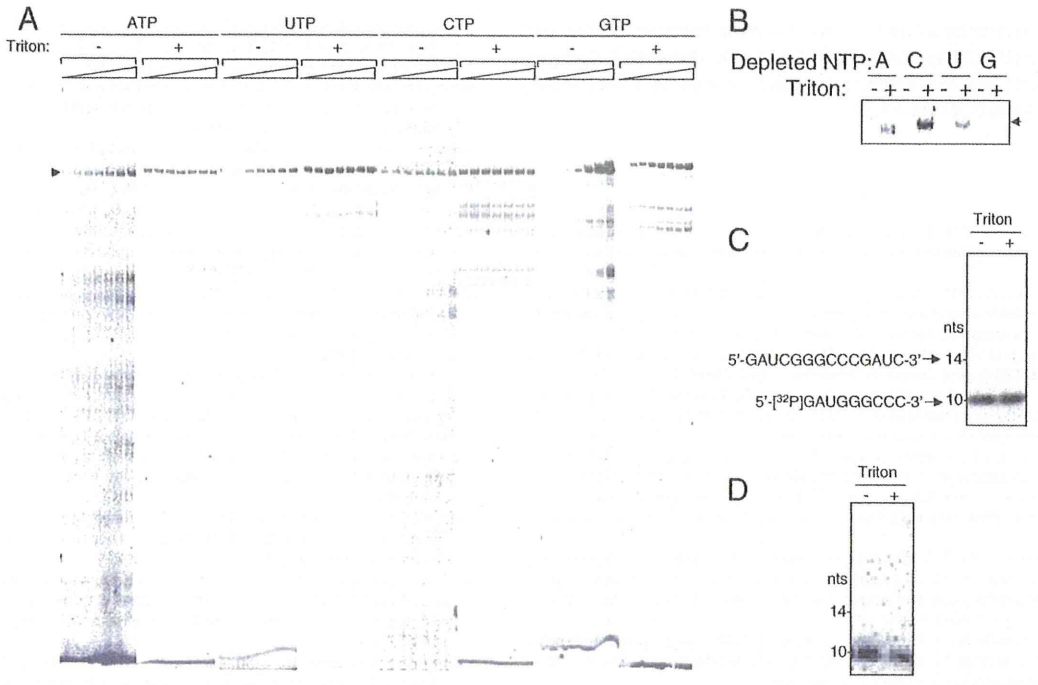

Fig. 7. Effect of substrate concentrations on in vitro transcription of HCR6 (1b) wild-type RNA polymerase, and TNTase activity in the presence of Triton X-100. A: Effect of nucleotide concentration on HCV HCR6 (1b) RdRpwt in vitro transcription with (+) and without (−) 0.02% Triton X-100. The concentration of ATP, UTP, and CTP varied from 1 to 50 μM, and that of GTP varied from 5 to 500 μM. B: Effect of nucleotide depletion on HCV HCR6 (1b) RdRpwt in vitro transcription with (+) and without (−) 0.02% Triton X-100. The position of 184-nt products is indicated by an arrowhead (A and B). C: TNTase activity of HCV HCR6 (1b) RdRpwt. 5′-[^{32}P]sym/sub was transcribed by HCV HCR6 (1b) RdRpwt with (+) and without (−) 0.02% Triton X-100. D: TNTase activity of HCV HCR6 (1b) RdRpwt. sym/sub was transcribed with [^{32}P]UTP by HCV HCR6 (1b) RdRpwt with (+) and without (−) 0.02% Triton X-100. The position of 10-nt sym/sub and 14-nt is indicated on the left.

RdRp which formed oligomer using 502H did not show high polymerase activity (Figs. 3–6). The inactive oligomer may be a part of the reason why a small fraction, less than 1%, of the purified HCV BK RdRp which belonged to 1b participated productively in transcription in vitro (Carroll et al., 2000). Taking together the data obtained by FRET (Clemente-Casares et al., 2011) and yeast two-hybrid systems (Wang et al., 2002), dynamic intermolecular interactions may occur under transcription conditions through the αT helix where amino acid 502 is located. The reason why only 1b RdRp was activated with Triton X-100 although RNA binding of all the RdRps tested was enhanced with Triton X-100, is not clear.

In case of JFH1 (2a) RdRp, the interaction with Triton X-100 may be different from that of HCR6 (1b) RdRp because it was not activated with Triton X-100 (Figs. 1 and 3), and because its gel-filtration profile was not affected with Triton X-100 (Fig. 5). This may be the reason of the inhibition of polymerase activity of JFH1 (2a) RdRpS502H by Triton X-100 although it was also disrupted to monomer (Figs. 3 and 6).

Triton X-100 activated only HCV 1b RdRp (Figs. 3 and 4). The closed conformation of HCV RdRp is required for de novo initiation (Chinnaswamy et al., 2008). With and without Triton X-100, JFH1 (2a) RdRpwt showed as high polymerase activity as HCR6 (1b) RdRpwt did with Triton X-100 (Fig. 3B). The very closed conformation of JFH1 (2a) RdRp is proposed to facilitate de novo initiation and high polymerase activity (Simister et al., 2009). Triton X-100 may also help the conformational change of HCR6 (1b) RdRp to the very closed conformation like that of JFH1 (2a) RdRp during transcription initiation.

HCV RdRp was co-purified with nucleic acids (Figs. S1 and S2). The contaminating nucleic acids were removed from HCV RdRp by high salt treatment. The contaminating nucleic acids carry proteins that have affinity to them, which misleads HCV in vitro transcription data. They also oligomerize HCV RdRp by crosslinking them. In a similar way, the contaminating nucleic acids in HCV RdRp preparations may mislead the binding data of HCV RdRp with other proteins.

From the activation kinetics of the detergents (Fig. 1, Table 1), the polymerase activation of 1b RdRp is likely to depend on the micelle formation of the detergent and on the direct interaction between RdRp and the detergents. The reason why the non-ionic detergent nOG did not activate the HCV RdRp is not known (Figs. 1 and 2).

The interaction mechanism of Triton X-100 and HCV 1b RdRp may be similar as that of sphingomyelin and HCV 1b RdRp because their activation kinetics were similar and the activated genotype was the same (Weng et al., 2010). Sphingomyelin activated only HCV 1b, but did not activate 1a or 2a RdRps. Both the activation curve of sphingomyelin and that of Triton X-100 showed the linear increase of polymerase activity. Then, sphingomyelin reached plateau at 20 molecules, and Triton X-100 reached plateau around its CMC.

Data about TNTase activity of HCV RdRp are controversial (Behrens et al., 1996; Ranjith-Kumar et al., 2001, 2004; Vo et al., 2004). In our system, TNTase activity was not detected with or without Triton X-100 (Figs. 7C and D).

GTP binds to HCV RdRp both as substrate and as a component of RdRp (Bressanelli et al., 2002). The apparent *Km* for GTP with Triton X-100 indicated that the substrate affinity dropped as low as to lose fidelity (Table 1, Figs. 7A and B). Triton X-100 may have affected the substrate-binding although its mechanism is not clear. HCV 1b full-length RdRp transcription activity obtained with CHAPS (Wang et al., 2002) might be that without fidelity as shown with Triton X-100. Detergents should not be used while screening substrate inhibitors of HCV RdRp. These data indicate that caution should be exercised while using detergents in anti-HCV RdRp drug screening tests.

Supplementary materials related to this article can be found online at doi:10.1016/j.gene.2012.01.044.

Acknowledgments

We thank Dr. J. Bukh, Dr. C. Rice, and Dr. R. Bartenshlager for providing pJ6CF, pHCVrepl3(S2204I)Neo, and Con1, respectively. This

work was supported by a Grant-in-Aid from the Chinese Academy of Sciences (O514P51131 and KSCX1-YW-10), the Chinese 973 Project (2009CB522504), and the Chinese National Science and Technology Major Project (2008ZX10002-014).

References

Aizaki, H., Lee, K.J., Sung, V.M., Ishiko, H., Lai, M.M., 2004. Characterization of the hepatitis C virus RNA replication complex associated with lipid rafts. Virology 324, 450–461.

Arnold, J.J., Cameron, C.E., 2000. Poliovirus RNA-dependent RNA polymerase (3D(pol)). Assembly of stable, elongation-competent complexes by using a symmetrical primer-template substrate (sym/sub). J. Biol. Chem. 275, 5329–5336.

Behrens, S.E., Tomei, L., De Francesco, R., 1996. Identification and properties of the RNA-dependent RNA polymerase of hepatitis C virus. EMBO J. 15, 12–22.

Binder, M., Quinkert, D., Bochkarova, O., Klein, R., Kezmic, N., Bartenschlager, R., Lohmann, V., 2007. Identification of determinants involved in initiation of hepatitis C virus RNA synthesis by using intergenotypic replicase chimeras. J. Virol. 81, 5270–5283.

Blight, K.J., McKeating, J.A., Marcotrigiano, J., Rice, C.M., 2003. Efficient replication of hepatitis C virus genotype 1a RNAs in cell culture. J. Virol. 77, 3181–3190.

Bressanelli, S., Tomei, L., Rey, F.A., De Francesco, R., 2002. Structural analysis of the hepatitis C virus RNA polymerase in complex with ribonucleotides. J. Virol. 76, 3482–3492.

Carroll, S.S., Sardana, V., Yang, Z., Jacobs, A.R., Mizenko, C., Hall, D., Hill, L., Zugay-Murphy, J., Kuo, L.C., 2000. Only a small fraction of purified hepatitis C RNA-dependent RNA polymerase is catalytically competent: implications for viral replication and in vitro assays. Biochemistry 39, 8243–8249.

Chinnaswamy, S., Murali, A., Li, P., Fujisaki, K., Kao, C.C., 2010. Regulation of de novo-initiated RNA synthesis in hepatitis C virus RNA-dependent RNA polymerase by intermolecular interactions. J. Virol. 84, 5923–5935.

Chinnaswamy, S., Yarbrough, I., Palaninathan, S., Kumar, C.T., Vijayaraghavan, V., Demeler, B., Lemon, S.M., Sacchettini, J.C., Kao, C.C., 2008. A locking mechanism regulates RNA synthesis and host protein interaction by the hepatitis C virus polymerase. J. Biol. Chem. 283, 20535–20546.

Clemente-Casares, P., Lopez-Jimenez, A.J., Bellon-Echeverria, I., Encinar, J.A., Martinez-Alfaro, E., Perez-Flores, R., Mas, A., 2011. De novo polymerase activity and oligomerization of hepatitis C virus RNA-dependent RNA-polymerases from genotypes 1 to 5. PLoS One 6, e18515.

Cramer, J., Jaeger, J., Restle, T., 2006. Biochemical and pre-steady-state kinetic characterization of the hepatitis C virus RNA polymerase (NS5BDelta21, HC-J4). Biochemistry 45, 3610–3619.

Fernandez-Recio, J., Vazquez, A., Civera, C., Sevilla, P., Sancho, J., 1997. The tryptophan/histidine interaction in alpha-helices. J. Mol. Biol. 267, 184–197.

Ferrari, E., Wright-Minogue, J., Fang, J.W., Baroudy, B.M., Lau, J.Y., Hong, Z., 1999. Characterization of soluble hepatitis C virus RNA-dependent RNA polymerase expressed in *Escherichia coli*. J. Virol. 73, 1649–1654.

Grakoui, A., McCourt, D.W., Wychowski, C., Feinstone, S.M., Rice, C.M., 1993. Characterization of the hepatitis C virus-encoded serine proteinase: determination of proteinase-dependent polyprotein cleavage sites. J. Virol. 67, 2832–2843.

Hijikata, M., Mizushima, H., Tanji, Y., Komoda, Y., Hirowatari, Y., Akagi, T., Kato, N., Kimura, K., Shimotohno, K., 1993. Proteolytic processing and membrane association of putative nonstructural proteins of hepatitis C virus. Proc. Natl. Acad. Sci. U. S. A. 90, 10773–10777.

Hirschman, S.Z., Gerber, M., Garfinkel, E., 1978. Differential activation of hepatitis B DNA polymerase by detergent and salt. J. Med. Virol. 2, 61–76.

Hong, Z., Cameron, C.E., Walker, M.P., Castro, C., Yao, N., Lau, J.Y., Zhong, W., 2001. A novel mechanism to ensure terminal initiation by hepatitis C virus NS5B polymerase. Virology 285, 6–11.

Kashiwagi, T., Hara, K., Kohara, M., Iwahashi, J., Hamada, N., Honda-Yoshino, H., Toyoda, T., 2002a. Promoter/origin structure of the complementary strand of hepatitis C virus genome. J. Biol. Chem. 277, 28700–28705.

Kashiwagi, T., Hara, K., Kohara, M., Kohara, K., Iwahashi, J., Hamada, N., Yoshino, H., Toyoda, T., 2002b. Kinetic analysis of C-terminally truncated RNA-dependent RNA polymerase of hepatitis C virus. Biochem. Biophys. Res. Commun. 290, 1188–1194.

Kiyosawa, K., Sodeyama, T., Tanaka, E., Gibo, Y., Yoshizawa, K., Nakano, Y., Furuta, S., Akahane, Y., Nishioka, K., Purcell, R.H., et al., 1990. Interrelationship of blood transfusion, non-A, non-B hepatitis and hepatocellular carcinoma: analysis by detection of antibody to hepatitis C virus. Hepatology 12, 671–675.

Lemon, S., Walker, C., Alter, M., Yi, M., 2007. Hepatitis C virus. In: Knipe, D., Howley, P. (Eds.), *Fields Virology*. Lippincott-Raven Publishers, Philadelphia, PA, pp. 1253–1304.

Lohmann, V., Korner, F., Herian, U., Bartenschlager, R., 1997. Biochemical properties of hepatitis C virus NS5B RNA-dependent RNA polymerase and identification of amino acid sequence motifs essential for enzymatic activity. J. Virol. 71, 8416–8428.

Luo, G., Hamatake, R.K., Mathis, D.M., Racela, J., Rigat, K.L., Lemm, J., Colonno, R.J. De, 2000. novo initiation of RNA synthesis by the RNA-dependent RNA polymerase (NS5B) of hepatitis C virus. J. Virol. 74, 851–863.

Marti, D.N., Bosshard, H.R., 2003. Electrostatic interactions in leucine zippers: thermodynamic analysis of the contributions of Glu and His residues and the effect of mutating salt bridges. J. Mol. Biol. 330, 621–637.

Matthews, J.M., Ward, L.D., Hammacher, A., Norton, R.S., Simpson, R.J., 1997. Roles of histidine 31 and tryptophan 34 in the structure, self-association, and folding of murine interleukin-6. Biochemistry 36, 6187–6196.

Murayama, A., Date, T., Morikawa, K., Akazawa, D., Miyamoto, M., Kaga, M., Ishii, K., Suzuki, T., Kato, T., Mizokami, M., Wakita, T., 2007. The NS3 helicase and NS5B-to-3′X regions are important for efficient hepatitis C virus strain JFH-1 replication in Huh7 cells. J. Virol. 81, 8030–8040.

Murayama, A., Weng, L., Date, T., Akazawa, D., Tian, X., Suzuki, T., Kato, T., Tanaka, Y., Mizokami, M., Wakita, T., Toyoda, T., 2010. RNA polymerase activity and specific RNA structure are required for efficient HCV replication in cultured cells. PLoS Pathog. 6, e1000885.

Qin, W., Luo, H., Nomura, T., Hayashi, N., Yamashita, T., Murakami, S., 2002. Oligomeric interaction of hepatitis C virus NS5B is critical for catalytic activity of RNA-dependent RNA polymerase. J. Biol. Chem. 277, 2132–2137.

Ranjith-Kumar, C.T., Gajewski, J., Gutshall, L., Maley, D., Sarisky, R.T., Kao, C.C., 2001. Terminal nucleotidyl transferase activity of recombinant Flaviviridae RNA-dependent RNA polymerases: implication for viral RNA synthesis. J. Virol. 75, 8615–8623.

Ranjith-Kumar, C.T., Sarisky, R.T., Gutshall, L., Thomson, M., Kao, C.C. De, 2004. novo initiation pocket mutations have multiple effects on hepatitis C virus RNA-dependent RNA polymerase activities. J. Virol. 78, 12207–12217.

Saito, I., Miyamura, T., Ohbayashi, A., Harada, H., Katayama, T., Kikuchi, S., Watanabe, Y., Koi, S., Onji, M., Ohta, Y., et al., 1990. Hepatitis C virus infection is associated with the development of hepatocellular carcinoma. Proc. Natl. Acad. Sci. U. S. A. 87, 6547–6549.

Sakamoto, H., Okamoto, K., Aoki, M., Kato, H., Katsume, A., Ohta, A., Tsukuda, T., Shimma, N., Aoki, Y., Arisawa, M., Kohara, M., Sudoh, M., 2005. Host sphingolipid biosynthesis as a target for hepatitis C virus therapy. Nat. Chem. Biol. 1, 333–337.

Schmitt, M., Scrima, N., Radujkovic, D., Caillet-Saguy, C., Simister, P.C., Friebe, P., Wicht, O., Klein, R., Bartenschlager, R., Lohmann, V., Bressanelli, S., 2011. A comprehensive structure–function comparison of hepatitis C virus strain JFH1 and J6 polymerases reveals a key residue stimulating replication in cell culture across genotypes. J. Virol. 85, 2565–2581.

Shi, S.T., Lee, K.J., Aizaki, H., Hwang, S.B., Lai, M.M., 2003. Hepatitis C virus RNA replication occurs on a detergent-resistant membrane that cofractionates with caveolin-2. J. Virol. 77, 4160–4168.

Simister, P., Schmitt, M., Geitmann, M., Wicht, O., Danielson, U.H., Klein, R., Bressanelli, S., Lohmann, V., 2009. Structural and functional analysis of hepatitis C virus strain JFH1 polymerase. J. Virol. 83, 11926–11939.

Takeuchi, H., Okada, A., Miura, T., 2003. Roles of the histidine and tryptophan side chains in the M2 proton channel from influenza A virus. FEBS Lett. 552, 35–38.

Tanaka, T., Kato, N., Cho, M.J., Sugiyama, K., Shimotohno, K., 1996. Structure of the 3′ terminus of the hepatitis C virus genome. J. Virol. 70, 3307–3312.

Thompson, F.M., Libertini, L.J., Joss, U.R., Calvin, M., 1972. Detergent effects on a reverse transcriptase activity and on inhibition by rifamycin derivatives. Science 178, 505–507.

Tsukiyama-Kohara, K., Iizuka, N., Kohara, M., Nomoto, A., 1992. Internal ribosome entry site within hepatitis C virus RNA. J. Virol. 66, 1476–1483.

Vo, N.V., Tuler, J.R., Lai, M.M., 2004. Enzymatic characterization of the full-length and C-terminally truncated hepatitis C virus RNA polymerases: function of the last 21 amino acids of the C terminus in template binding and RNA synthesis. Biochemistry 43, 10579–10591.

Wang, Q.M., Hockman, M.A., Staschke, K., Johnson, R.B., Case, K.A., Lu, J., Parsons, S., Zhang, F., Rathnachalam, R., Kirkegaard, K., Colacino, J.M., 2002. Oligomerization and cooperative RNA synthesis activity of hepatitis C virus RNA-dependent RNA polymerase. J. Virol. 76, 3865–3872.

Wasley, A., Alter, M.J., 2000. Epidemiology of hepatitis C: geographic differences and temporal trends. Semin. Liver Dis. 20, 1–16.

Watashi, K., Ishii, N., Hijikata, M., Inoue, D., Murata, T., Miyanari, Y., Shimotohno, K., 2005. Cyclophilin B is a functional regulator of hepatitis C virus RNA polymerase. Mol. Cell 19, 111–122.

Weng, L., Du, J., Zhou, J., Ding, J., Wakita, T., Kohara, M., Toyoda, T., 2009. Modification of hepatitis C virus 1b RNA polymerase to make a highly active JFH1-type polymerase by mutation of the thumb domain. Arch. Virol. 154, 765–773.

Weng, L., Hirata, Y., Arai, M., Kohara, M., Wakita, T., Watashi, K., Shimotohno, K., He, Y., Zhong, J., Toyoda, T., 2010. Sphingomyelin activates hepatitis C virus RNA polymerase in a genotype specific manner. J. Virol. 84, 11761–11770.

Weyant, R.S., Edmonds, P., Swaminathan, B., 1990. Effect of ionic and nonionic detergents on the Taq polymerase. Biotechniques 9, 308–309.

Wu, A.M., Cetta, A., 1975. On the stimulation of viral DNA polymerase activity by nonionic detergent. Biochemistry 14, 789–795.

Journal of Virology

Production of Infectious Chimeric Hepatitis C Virus Genotype 2b Harboring Minimal Regions of JFH-1

Asako Murayama, Takanobu Kato, Daisuke Akazawa, Nao Sugiyama, Tomoko Date, Takahiro Masaki, Shingo Nakamoto, Yasuhito Tanaka, Masashi Mizokami, Osamu Yokosuka, Akio Nomoto and Takaji Wakita

***J. Virol.* 2012, 86(4):2143. DOI: 10.1128/JVI.05386-11.**
Published Ahead of Print 7 December 2011.

JVI
Journals.ASM.org

Production of Infectious Chimeric Hepatitis C Virus Genotype 2b Harboring Minimal Regions of JFH-1

Asako Murayama,[a] Takanobu Kato,[a] Daisuke Akazawa,[a] Nao Sugiyama,[a] Tomoko Date,[a] Takahiro Masaki,[a] Shingo Nakamoto,[b] Yasuhito Tanaka,[c] Masashi Mizokami,[d] Osamu Yokosuka,[b] Akio Nomoto,[e]* and Takaji Wakita[a]

Department of Virology II, National Institute of Infectious Diseases, Shinjuku-ku, Tokyo, Japan[a]; Department of Medicine and Clinical Oncology, Graduate School of Medicine, Chiba University, Chuo, Chiba, Japan[b]; Department of Virology and Liver Unit, Nagoya City University Graduate School of Medical Sciences, Kawasumi, Mizuho, Nagoya, Japan[c]; The Research Center for Hepatitis and Immunology, National Center for Global Health and Medicine, Ichikawa, Chiba, Japan[d]; and Department of Microbiology, Graduate School of Medicine, University of Tokyo, Bunkyo-ku, Tokyo, Japan[e]

To establish a cell culture system for chimeric hepatitis C virus (HCV) genotype 2b, we prepared a chimeric construct harboring the 5′ untranslated region (UTR) to the E2 region of the MA strain (genotype 2b) and the region of p7 to the 3′ UTR of the JFH-1 strain (genotype 2a). This chimeric RNA (MA/JFH-1.1) replicated and produced infectious virus in Huh7.5.1 cells. Replacement of the 5′ UTR of this chimera with that from JFH-1 (MA/JFH-1.2) enhanced virus production, but infectivity remained low. In a long-term follow-up study, we identified a cell culture-adaptive mutation in the core region (R167G) and found that it enhanced virus assembly. We previously reported that the NS3 helicase (N3H) and the region of NS5B to 3′ X (N5BX) of JFH-1 enabled replication of the J6CF strain (genotype 2a), which could not replicate in cells. To reduce JFH-1 content in MA/JFH-1.2, we produced a chimeric viral genome for MA harboring the N3H and N5BX regions of JFH-1, combined with a JFH-1 5′ UTR replacement and the R167G mutation (MA/N3H+N5BX-JFH1/R167G). This chimeric RNA replicated efficiently, but virus production was low. After the introduction of four additional cell culture-adaptive mutations, MA/N3H+N5BX-JFH1/5am produced infectious virus efficiently. Using this chimeric virus harboring minimal regions of JFH-1, we analyzed interferon sensitivity and found that this chimeric virus was more sensitive to interferon than JFH-1 and another chimeric virus containing more regions from JFH-1 (MA/JFH-1.2/R167G). In conclusion, we established an HCV genotype 2b cell culture system using a chimeric genome harboring minimal regions of JFH-1. This cell culture system may be useful for characterizing genotype 2b viruses and developing antiviral strategies.

Hepatitis C virus (HCV) is a major cause of chronic liver disease (5, 13), but the lack of a robust cell culture system to produce virus particles has hampered the progress of HCV research (2). Although the development of a subgenomic replicon system has enabled research into HCV RNA replication (15), infectious virus particle production has not been possible. Recently, an HCV cell culture system was developed using a genotype 2a strain, JFH-1, cloned from a fulminant hepatitis patient (14, 29, 32), thereby allowing investigation of the entire life cycle of this virus. However, several groups of investigators have reported genotype- and/or strain-dependent effects of some antiviral reagents (6, 17) and neutralizing antibodies (7, 25). Therefore, efficient virus production systems using various genotypes and strains are indispensable for HCV research and the development of antiviral strategies.

The JFH-1 strain is the first HCV strain that can efficiently produce HCV particles in HuH-7 cells (29). Other strains can replicate and produce infectious virus by HCV RNA transfection, but the efficiency is far lower than that of JFH-1 (24, 31). In the case of replication-incompetent strains, chimeric virus containing the JFH-1 nonstructural protein coding region is useful for analyses of viral characteristics (6, 9, 14, 23, 30, 31).

In this study, we developed a genotype 2b chimeric infectious virus production system using the MA strain (accession number AB030907) (19) harboring minimal regions of JFH-1 and cell culture-adaptive mutations that enhance infectious virus production.

MATERIALS AND METHODS

Cell culture. Huh7.5.1 cells (a kind gift from Francis V. Chisari) (32) and Huh7-25 cells (1) were cultured at 37°C in Dulbecco's modified Eagle's medium containing 10% fetal bovine serum under 5% CO_2 conditions. For follow-up study, RNA-transfected cells were passaged every 2 to 5 days depending on cell status.

Full-length genomic HCV constructs. Plasmids used in the analysis of genomic RNA replication were constructed based on pJFH1 (29) and pMA (19). For convenience, an EcoRI recognition site was introduced upstream of the T7 promoter region of pMA by PCR, and an XbaI recognition site was introduced at the end of the 3′ untranslated region (UTR). To construct MA/JFH-1, the EcoRI-BsaBI (nucleotides [nt] 1 to 2570; 5′ UTR to E2) fragment of pMA was substituted into pJFH1 (Fig. 1A). Replacement of the 5′ UTR was performed by exchanging the EcoRI-AgeI (nt 1 to 159) fragment. A point mutation in the core region (R167G) was introduced into MA chimeric constructs by PCR using the following primers: sense, 5′-TTA TGC AAC GGG GAA TTT ACC CGG TTG CTC T-3′; antisense, 5′-GGT AAA TTC CCC GTT GCA TAA TTT ATC CCG TC-3′. G167R substitution in the JFH-1 construct was performed by PCR using the following primers: sense, 5′-ATT ATG CAA CAA GGA ACC TAC CCG GTT TCC C-3′; antisense, 5′-GGT AGG TTC CTT GTT GCA TAA TTA ACC CCG TC-3′. Point mutations (L814S, R1012G, T1106A, and V1951A) were introduced into MA chimeric constructs by PCR using the following primers: L814S, 5′-GCT TAC GCC TCG GAC GCC GCT GAA CAA GGG G-3′ (sense) and 5′-AGC GGC GTC CGA GGC GTA AGC CTG CTG CGG C-3′ (antisense); R1012G, 5′-GAG GCT AGG TGG

Received 13 June 2011 Accepted 23 November 2011
Published ahead of print 7 December 2011
Address correspondence to Takaji Wakita, wakita@nih.go.jp.
* Present address: Institute of Microbial Chemistry, Shinagawa-ku, Tokyo, Japan.

doi:10.1128/JVI.05386-11

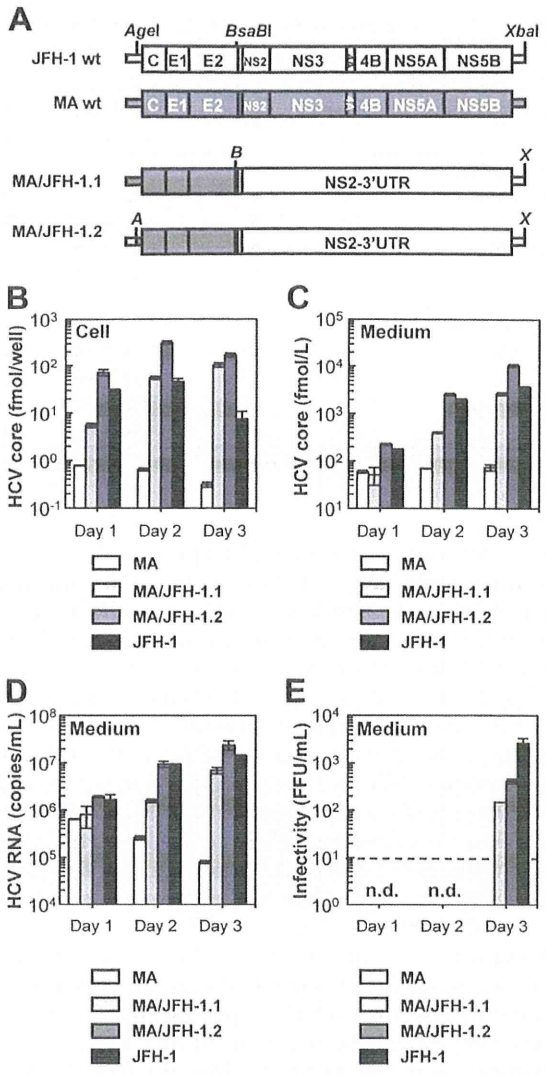

FIG 1 Replication and virus production by MA/JFH-1 chimeras in Huh7.5.1 cells. (A) Schematic structures of JFH-1, MA, and two MA/JFH-1 chimeras (MA/JFH-1.1 and MA/JFH-1.2). The junction of JFH-1 and MA in the 5′ UTR is an AgeI site, and the junction of MA and JFH-1 in the NS2 region is a BsaBI site. A, AgeI; B, BsaBI; X, XbaI. (B to E) Chimeric HCV RNA replication in Huh7.5.1 cells. HCV core protein level in cells (B) and culture medium (C) and HCV RNA levels in medium (D) and infectivity of culture medium (E) from HCV RNA-transfected Huh7.5.1 cells are shown. Ten micrograms of HCV RNA was transfected into Huh7.5.1 cells, and cells and culture medium were harvested on days 1, 2, and 3. n.d., not determined. Assays were performed three times independently, and data are presented as means ± standard deviation. Dashed line indicates detection limit. wt, wild type.

GGA AGT TCT GCT CGG CCC T-3′ (sense) and 5′-AGA ACT TCC CCA CCT AGC CTC GCG GAA ACC G-3′ (antisense); T1106A, 5′-CAG ATG TAC GCC AGC GCA GAG GGG GAC CTC-3′ (sense) and 5′-CTG CGC TGG CGT ACA TCT GGG TGA CTG GTC-3′ (antisense); and V1951A, 5′-GTG ACG CAG GCG TTA AGC TCA CTC ACA ATT ACC-3′ (sense) and 5′-TGA GCT TAA CGC CTG CGT CAC GCG CAG CGA G-3′ (antisense). To construct the MA chimeric virus harboring minimal regions of JFH-1 (MA/N3H+N5BX-JFH1), ClaI (nt 3930), EcoT22I (nt 5294), and BsrGI (nt 7782) recognition sites were introduced into pMA by site-directed mutagenesis. The 5′ UTR (EcoRI-AgeI), the region of the NS3 helicase (N3H; ClaI-EcoT22I), and the region of NS5B to 3′ X (N5BX; BsrGI-XbaI) were then replaced with the corresponding regions from JFH-1.

RNA synthesis, transfection, and determination of infectivity. RNA synthesis and transfection were performed as described previously (12, 22). Determination of infectivity was also performed as described previously, with infectivity expressed as the number of focus-forming units per milliliter (FFU/ml) (12, 22). When necessary, culture medium was concentrated 20-fold in Amicon Ultra-15 spin columns (100-kDa molecular-weight-cutoff; Millipore, Bedford, MA) in order to determine infectivity.

Quantification of HCV core protein and HCV RNA. In order to estimate the concentration of HCV core protein in culture medium, we performed a chemiluminescence enzyme immunoassay (Lumipulse II HCV core assay; Fujirebio, Tokyo, Japan) in accordance with the manufacturer's instructions. HCV RNA from harvested cells or culture medium was isolated using an RNeasy Mini RNA kit (Qiagen, Tokyo, Japan) or QiaAmp Viral RNA Minikit (Qiagen), respectively. Copy number of HCV RNA was determined by real-time quantitative reverse transcription-PCR (qRT-PCR), as described previously (28).

HCV sequencing. Total RNA in culture supernatant was extracted with Isogen-LS (Nippon Gene Co., Ltd., Tokyo, Japan). cDNA was synthesized using Superscript III Reverse Transcriptase (Invitrogen, Carlsbad, CA). cDNA was subsequently amplified with LA *Taq* DNA polymerase (TaKaRa, Shiga, Japan). Four separate PCR primer sets were used to amplify the fragments of nt 130 to 2909, 2558 to 5142, 4784 to 7279, and 7081 to 9634 covering the entire open reading frame and part of the 5′ UTR and 3′ UTR of the MA strain. Sequences of amplified fragments were determined directly.

Immunostaining. Infected cells were cultured on Multitest Slides (MP Biomedicals, Aurora, OH) and were fixed in acetone-methanol (1:1, vol/vol) for 15 min at −20°C. After a blocking step, infected cells were visualized with anti-core protein antibody (clone 2H9) (29) and Alexa Fluor 488 goat anti-mouse IgG (Invitrogen), and nuclei were visualized with 4′,6′-diamidino-2-phenylindole (DAPI).

Assessment of interferon sensitivity. Two micrograms of *in vitro* transcribed RNA was transfected into 3×10^6 Huh7.5.1 cells. Four hours after transfection, cells were placed in fresh medium or medium containing 0.1, 1, 10, 100, and 1,000 IU/ml of interferon α-2b (Intron A; Schering-Plough Corporation, Osaka, Japan). Culture medium was then harvested on day 3, and HCV core levels in the cells and in the medium were measured.

Statistical analysis. Significant differences were evaluated by Student's *t* test. A *P* value of <0.05 was considered significant.

RESULTS

Transient replication and production of 2b/2a chimeric virus. We first tested whether the MA strain (genotype 2b) (19) was able to replicate and produce infectious virus in cultured cells. When the *in vitro* transcribed RNA of MA was transfected into Huh7.5.1 cells, a highly HCV-permissive cell line, replication and virus production were not observed (Fig. 1A to C). We then tested whether 2b/2a chimeric RNA harboring the structural region (5′ UTR to E2) of the MA strain and the nonstructural region (p7 to 3′ UTR) of JFH-1 (Fig. 1A, MA/JFH-1.1) was able to replicate in the cells. After MA/JFH-1.1 RNA transfection, time-dependent accumulation of core protein in the cells (Fig. 1B) and culture medium (Fig. 1C) was observed, indicating that MA/JFH-1.1 RNA was able to replicate in the cells autonomously. HCV RNA levels in the medium were determined by qRT-PCR, and time-dependent increases in HCV RNA level were also observed (Fig. 1D). Infectious virus production was observed on day 3, but infectivity was 17.6-fold lower than that of JFH-1 (Fig. 1E).

In order to improve the level of infectious virus production, we tested another chimeric construct, MA/JFH-1.2, which contained an additional MA-to-JFH-1 replacement of the 5′ UTR (Fig. 1A),

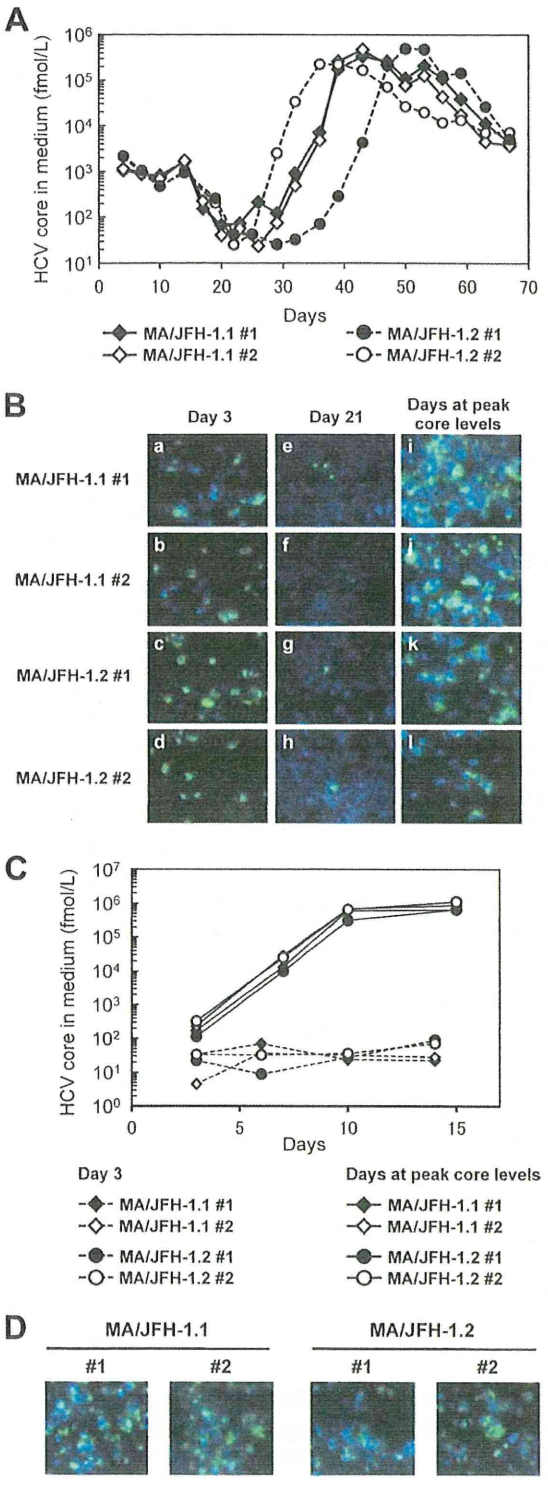

FIG 2 Long-term culture of MA/JFH-1.1 and MA/JFH-1.2 RNA-transfected cells. Ten micrograms of HCV RNA was transfected into Huh7.5.1 cells, and cells were passaged every 2 to 5 days, depending on cell status. Culture medium was collected after every passage, and HCV core protein levels were measured. Transfection was performed twice for each chimeric RNA (1 and 2 for each construct). (A) HCV core protein levels in culture medium from MA/JFH-1.1 and MA/JFH-1.2 RNA-transfected cells. (B) Immunostained cells at 3 days after transfection (a to d), at 21 days after transfection (e to h), and at the time of peak core levels (days 42 to 49). Infected cells were visualized with anti-core protein antibody (green), and nuclei were visualized with DAPI (blue). (C) Infection of naïve cells by culture medium at an MOI of 0.001. (D) Immunostained cells at 15 days after infection with medium at peak core protein levels (Fig. 2A) at an MOI of 0.001. Infected cells were visualized with anti-core antibody (green), and nuclei were visualized with DAPI (blue).

TABLE 1 HCV core protein levels and infectivity in culture medium immediately after RNA transfection (day 3) and after long-term culture (days 35 to 49)

Sample period and virus	Sample no.	Day no.[a]	HCV core (fmol/liter)	Infectivity (FFU/ml)
After transfection				
MA/JFH-1.1	1	3	1.06×10^3	5.00×10^1
	2	3	1.14×10^3	5.70×10^1
MA/JFH-1.2	1	3	2.14×10^3	7.30×10^1
	2	3	2.15×10^3	9.30×10^1
After long-term culture				
MA/JFH-1.1	1	42	3.38×10^5	1.62×10^5
	2	42	4.70×10^5	3.23×10^5
MA/JFH-1.2	1	35	2.27×10^5	1.61×10^5
	2	49	4.93×10^5	3.27×10^5

[a] For the long-term culture, the days are those of peak core protein levels.

as a 5′ UTR replacement from J6CF (genotype 2a) to JFH-1 enhanced virus production of chimeric J6CF virus harboring the region of NS2 to 3′ X of JFH-1 (J6/JFH-1) (A. Murayama et al., unpublished data). The core protein accumulation levels with MA/JFH-1.2 RNA-transfected cells were higher than those with MA/JFH-1.1 ($P < 0.05$) (Fig. 1B). Similarly, core protein and HCV RNA levels in the medium of MA/JFH-1.2 RNA-transfected cells were higher than those of MA/JFH-1.1 ($P < 0.05$) (Fig. 1C and D). Infectivity on day 3 was also higher than with MA/JFH-1.1 ($P < 0.05$) (Fig. 1E), indicating that the 5′ UTR of JFH-1 enhanced virus production. However, infectivity of medium from MA/JFH-1.2 RNA-transfected cells on day 3 remained 6.4-fold lower than that of JFH-1 although HCV RNA levels in the medium were similar to those of JFH-1 (Fig. 1D and E).

These results indicate that 2b/2a chimeric RNA is able to replicate autonomously in Huh7.5.1 cells and produce infectious virus although infectivity remains lower than that of JFH-1.

Assembly-enhancing mutation in core region introduced during long-term culture. Because MA/JFH-1.1 and MA/JFH-1.2 replicated efficiently but produced small amounts of infectious virus, we performed long-term culture of these RNA-transfected cells in order to examine whether these chimeric RNAs would continue replicating and producing infectious virus over the long term. We prepared two RNA-transfected cell lines for each construct (MA/JFH-1.1 and MA/JFH-1.2) as both of these replicated and produced infectious virus at different levels.

Immediately after transfection, core protein levels and infectivity in culture medium were low (1.06×10^3 to 2.15×10^3 fmol/liter and 5.00×10^1 to 9.30×10^1 FFU/ml, respectively) (Fig. 2A and Table 1) although a considerable number of core protein-positive cells were observed by immunostaining (Fig. 2B, frames a to d). Subsequently, core protein levels in the culture medium decreased gradually (Fig. 2A), and core protein-positive cells were rare (Fig. 2B, frames e to h). However, at 30 to 40 days

after transfection, core protein levels in the supernatants of all chimeric RNA-transfected cells increased and reached 2.27×10^5 to 4.93×10^5 fmol/liter (Fig. 2A and Table 1). Infectivity in the culture medium also increased (1.61×10^5 to 3.27×10^5 FFU/ml) (Table 1), and at this point, most of the cells were core protein positive (Fig. 2B, frame i to l).

As the infectivity of culture supernatant of MA/JFH-1 RNA-transfected cells appeared to increase after long-term culture, we compared viral spread by infection with these supernatants on day 3 (immediately after transfection) and for each peak in core protein levels (after long-term culture). When naïve Huh7.5.1 cells were infected with supernatant on days corresponding to a peak in core protein levels at a multiplicity of infection (MOI) of 0.001, core protein levels in the medium increased rapidly and reached 0.64×10^6 to 1.13×10^6 fmol/liter by day 15 after infection (Fig. 2C). Immunostained images showed that most cells were HCV core protein positive on day 15 (Fig. 2D). When naïve Huh7.5.1 cells were infected with supernatant from day 3 at an MOI of 0.001, core protein levels in the medium did not increase under these conditions (Fig. 2C). These results indicate that both MA/JFH-1 chimeric viruses (MA/JFH-1.1 and MA/JFH-1.2) acquired the ability to spread rapidly after long-term culture.

As the characteristics of the MA/JFH-1 virus changed in long-term culture, we analyzed the possible mutations in the viral genome from the supernatant at each peak in core protein levels (Table 1, days at peak core levels). Nine- to 12-nucleotide mutations were found in the viral genome from each supernatant, and the detected mutations were distributed along the entire genome. Among these mutations, a common nonsynonymous mutation was found in the core region (Arg to Gly at amino acid [aa]167, R167G).

In order to test the effects of R167G on virus production, an R167G substitution was introduced into MA/JFH-1.2 as MA/JFH-1.2 replicated and produced infectious virus more efficiently than MA/JFH-1.1. HCV core protein levels in cells and medium of MA/JFH-1.2 with R167G (MA/JFH-1.2/R167G) were higher than with MA/JFH-1.2 ($P < 0.05$) (Fig. 3A and B). HCV RNA levels in the medium of MA/JFH-1.2/R167G RNA-transfected cells were also higher than with MA/JFH-1.2 ($P < 0.05$) (Fig. 3C). Infectious virus production was also increased by the R167G mutation ($P < 0.05$) (Fig. 3D) and was 8.7-fold higher than that of JFH-1 RNA-transfected cells on day 3 ($P < 0.05$) (Fig. 3D).

We then tested whether R167G was responsible for the rapid spread observed in culture supernatant after long-term culture by monitoring virus spread after infection of naïve Huh7.5.1 with culture medium taken 3 days after RNA transfection of MA/JFH-1.2 and MA/JFH-1.2/R167G at an MOI of 0.005. Core protein levels in medium from MA/JFH-1.2/R167G-infected cells increased with the same kinetics as levels of JFH-1 (Fig. 3E), and the population of core protein-positive cells was almost the same as with JFH-1-infected cells (Fig. 3F), indicating that MA/JFH-1.2/R167G virus spread as rapidly as JFH-1 virus. In contrast, we observed no infectious foci in the MA/JFH-1.2 virus-inoculated cells (Fig. 3F). These data suggest that the R167G mutation in the core region was a cell culture-adaptive mutation and that it enhanced infectious MA/JFH-1.2 virus production.

In order to determine whether R167G enhances RNA replication or other steps in the viral life cycle, we performed a single-cycle virus production assay (11) using Huh7-25 cells, a HuH-7-derived cell line lacking CD81 expression on the cell surface (1).

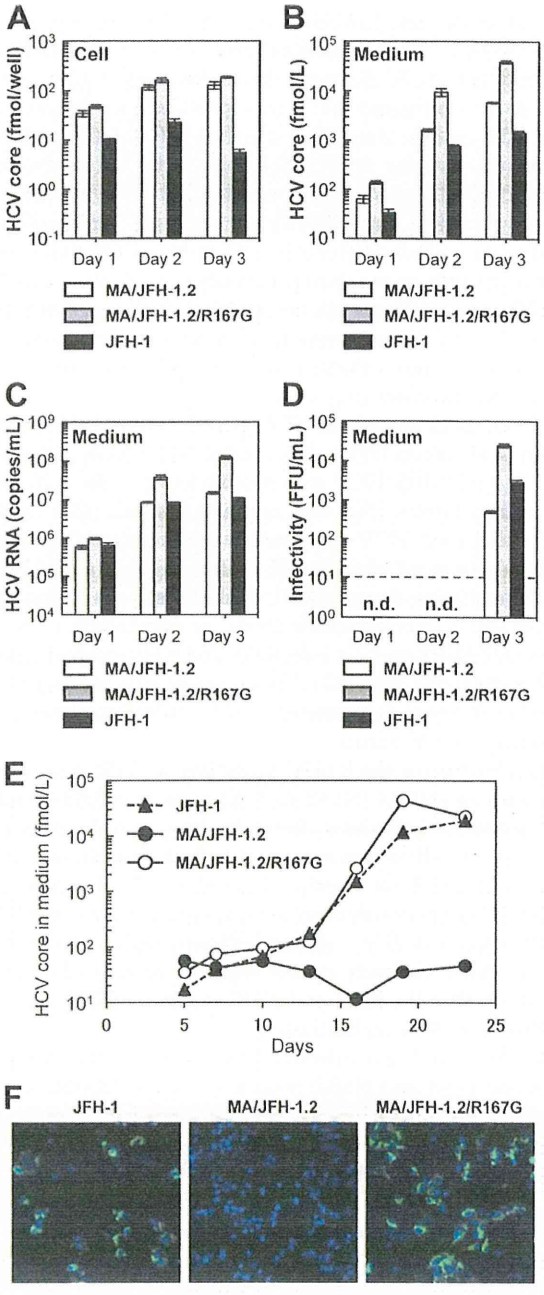

FIG 3 Effects of R167G on replication and virus production of MA/JFH-1.2 in Huh7.5.1 cells. Ten micrograms of HCV RNA was transfected into Huh7.5.1 cells, and cells and medium were harvested on days 1, 2, and 3. HCV core protein levels in the cells (A) and culture medium (B) and HCV RNA levels in the medium (C) and the infectivity of culture medium (D) from HCV RNA-transfected Huh7.5.1 cells are shown. n.d., not determined. Dashed line indicates the detection limit. Assays were performed three times independently, and data are presented as means ± standard deviation. (E) HCV core protein levels in culture medium from cells infected with medium at 3 days posttransfection at an MOI of 0.005. (F) Immunostained cells at 19 days postinfection. Infected cells were visualized with anti-core antibody (green), and nuclei were visualized with DAPI (blue).

This cell line can support replication and infectious virus production upon transfection of HCV genomic RNA but cannot be reinfected by progeny virus, thereby allowing observation of a single cycle of infectious virus production without the confounding ef-

fects of reinfection. R167G did not affect HCV core protein levels in the chimeric RNA-transfected Huh7-25 cells (Fig. 4A), demonstrating that R167G did not enhance RNA replication. Nevertheless, R167G increased HCV core protein levels in the medium ($P < 0.05$ on days 2 and 3) and infectivity (Fig. 4B and C). These results suggest that R167G did not affect RNA replication but affected other steps such as virus assembly and/or virus secretion.

Virus particle assembly efficiency was then assessed by determining intracellular-specific infectivity from infectivity and RNA titer in the cells, as reported previously (11). As shown in Fig. 4G, R167G enhanced intracellular-specific infectivity of MA/JFH-1.2 virus 10.2-fold. Virus secretion efficiency was also calculated from the amount of intracellular and extracellular infectious virus, but R167G had no effect (Fig. 4G).

To confirm the effects of Arg167 in other HCV strains, we tested its effects on JFH-1. As aa 167 of JFH-1 is Gly, we replaced it with Arg (G167R). HCV core protein levels in the cells were not affected by G167R (Fig. 4D), and no effects on RNA replication were confirmed. HCV core protein levels in the medium and infectivity decreased after G167R mutation (Fig. 4E and F). As the G167R mutation decreased intracellular infectious virus production of JFH-1 to undetectable levels, we were unable to determine the intracellular-specific infectivity and virus secretion efficiency of JFH-1 G167R (Fig. 4G). These results indicate that Gly is favored over Arg at core position 167 for infectious virus assembly in multiple HCV strains.

MA harboring the R167G mutation, 5′ UTR, and N3H (NS3 helicase) and N5BX (NS5B to 3′ X) regions of JFH-1 replicated and produced infectious chimeric virus. In order to establish a genotype 2b cell culture system with the MA strain with minimal regions of JFH-1, we attempted to reduce JFH-1 content in MA/JFH-1.2. We previously reported that replacement of the N3H and N5BX regions of JFH-1 allowed efficient replication of the J6CF strain, which normally cannot replicate in cells (21). Thus, we tested whether the N3H and N5BX regions of JFH-1 could also support MA RNA replication.

We prepared two chimeric MA constructs harboring the 5′ UTR and N3H and N5BX regions of JFH-1, MA/N3H+N5BX-JFH1 (Fig. 5A) and MA/N3H+N5BX-JFH1/R167G. After *in vitro* transcribed RNA was transfected into Huh7.5.1 cells, intracellular core protein levels of MA/N3H+N5BX-JFH1 and MA/N3H+N5BX-JFH1/R167G RNA-transfected cells increased in a time-dependent manner and reached almost the same levels as with MA/JFH-1.2 RNA-transfected cells on day 5 (Fig. 5B). Extracellular core protein and HCV RNA levels of MA/N3H+N5BX-JFH1 and MA/N3H+N5BX-JFH1/R167G RNA-transfected cells also increased in a time-dependent manner (Fig. 5C and D). However, they were more than 10 times lower than with MA/JFH-1.2 RNA-transfected cells although intracellular core levels were comparable on day 5 (Fig. 5B to D).

We then tested whether the medium from MA/N3H+N5BX-JFH1 and MA/N3H+N5BX-JFH1/R167G RNA-transfected cells was infectious. Infectivity of the medium from MA/N3H+N5BX-JFH1 RNA-transfected cells was below the detection limit, and that of MA/N3H+N5BX-JFH1/R167G RNA-transfected cells on day 5 was very low ($3.3 \times 10^1 \pm 2.1 \times 10^1$ FFU/ml) (Fig. 5E). To confirm infectivity, the culture media were concentrated, and their infectivity was determined. Infected foci were observed after infection with concentrated medium in MA/N3H+N5BX-JFH1/R167G RNA-transfected cells (Fig. 5F), and infectivity was found

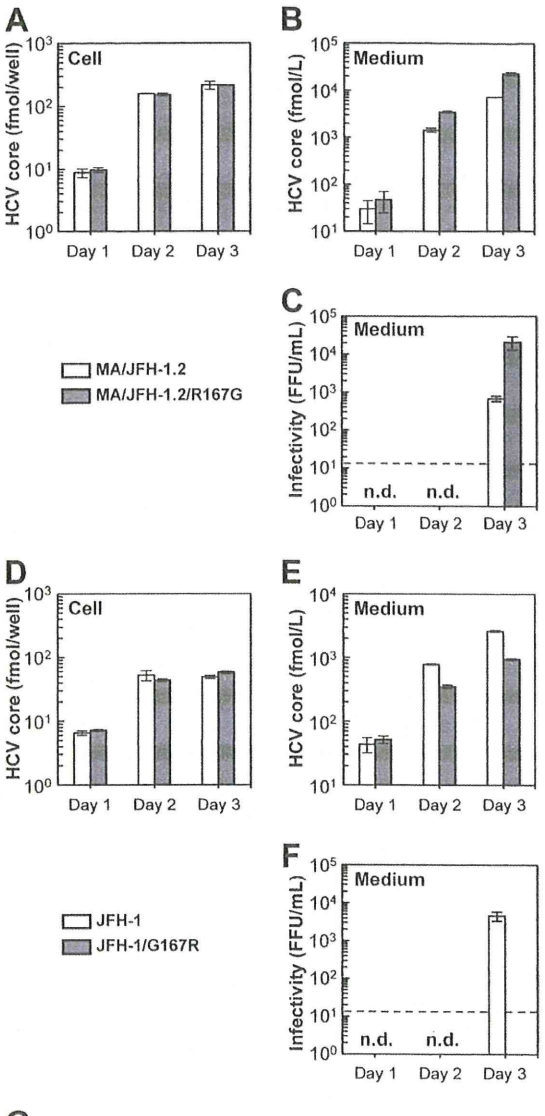

G

Construct	Intracellular Specific Infectivity (FFU/ x10^5 HCV RNA copies)	Infectious Virus Secretion (Extra/Intra)
MA/JFH-1.2	1.68 ± 0.404	20.2 ± 4.26
MA/JFH-1.2/R167G	17.1 ± 4.38	14.1 ± 1.65
JFH-1	1.78 ± 0.364	63.3 ± 6.44
JFH-1/G167R	NA	NA

FIG 4 Effects of R167G on replication and virus production of MA/JFH-1.2 and JFH-1 in Huh7-25 cells. Ten micrograms of HCV RNA was transfected into Huh7-25 cells, and cells and medium were harvested on days 1, 2, and 3. HCV core protein levels in cells (A and D) and in medium (B and E) were measured, and infectivity of medium (C and F) was determined. n.d., not determined. Dashed line indicates the detection limit. (G) Intracellular specific infectivity and virus secretion efficiency of chimeric HCV RNA-transfected cells. Intracellular and extracellular infectivity of day 3 samples was determined, and specific infectivity and virus secretion rate were calculated. Assays were performed three times independently, and data are presented as means ± standard deviation. NA, not available.

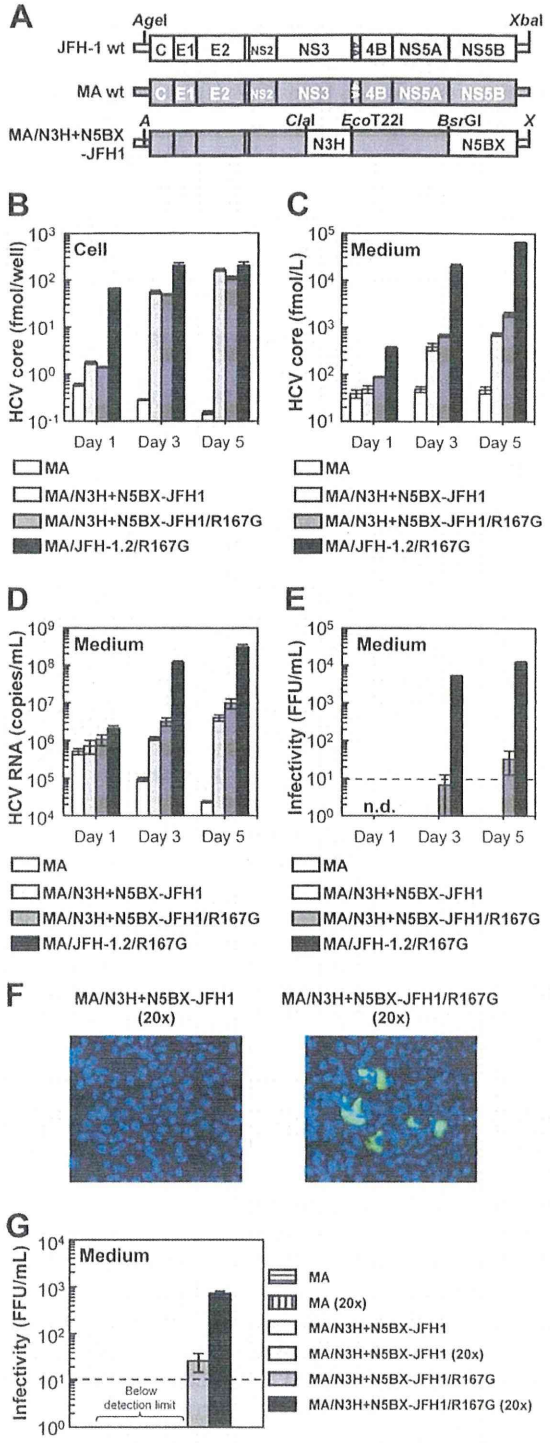

FIG 5 Replication and virus production of MA/N3H+N5BX-JFH1/R167G in Huh7.5.1 cells. (A) Schematic structures of JFH-1, MA, and MA/N3H+N5BX-JFH1. The junction of JFH-1 and MA in the 5′ UTR is an AgeI site; the junctions of MA and JFH-1 in the NS3 regions are ClaI and EcoT22I sites, and the junction in the NS5B region is a BsrGI site. A, AgeI; X, XbaI. (B to G) Chimeric HCV RNA replication in Huh7.5.1 cells. Ten micrograms of HCV RNA was transfected into Huh7.5.1 cells, and cells and medium were harvested on days 1, 3, and 5. HCV core protein levels in cells (B) and in medium (C) and HCV RNA levels in medium (D) were measured, and infectivity of medium (E) was determined. Assays were performed three times independently, and data are presented as means ± standard deviation. n.d., not determined. Dashed line indicates the detection limit. (F) Immunostained cells. Huh7.5.1 cells were infected with concentrated medium from RNA-transfected cells on day 5. Infected cells were visualized with anti-core antibody (green), and nuclei were visualized with DAPI (blue). (G) Infectivity of concentrated culture medium from HCV RNA-transfected cells. Culture medium was concentrated by 20 times. Infectivities of original and concentrated culture media were determined. Dashed line indicates detection thelimit.

to be $7.27 \times 10^2 \pm 7.57 \times 10^1$ FFU/ml (Fig. 5G). No infected foci were observed after infection of MA/N3H+N5BX-JFH1 RNA-transfected cells, even when medium was concentrated (Fig. 5F), although intracellular and extracellular core protein levels were comparable to those with MA/N3H+N5BX-JFH1/R167G RNA-transfected cells (Fig. 5B and C). These results indicate that replacement of the 5′ UTR and N3H and N5BX regions in JFH-1 were necessary to rescue autonomous replication in the replication-incompetent MA strain and for secretion of infectious chimeric virus. However, the secretion and infection efficiencies of the virus were low.

Cell culture-adaptive mutations enhanced infectious virus production of MA/N3H+N5BX-JFH1/R167G. Because MA/N3H+N5BX-JFH1/R167G replicated efficiently but produced very small amounts of infectious virus, we performed a long-term culture of the RNA-transfected cells in order to induce cell culture-adaptive mutations that could enhance infectious virus production. We prepared RNA-transfected cells using two constructs, MA/N3H+N5BX-JFH1 and MA/N3H+N5BX-JFH1/R167G; both of these replicated efficiently, and MA/N3H+N5BX-JFH1/R167G produced infectious virus at low levels while MA/N3H+N5BX-JFH1 did not. Immediately after transfection, the HCV core protein levels in the medium of each RNA-transfected cell culture peaked at 3.0×10^3 fmol/liter and declined thereafter. However, the core protein level in the medium with MA/N3H+N5BX-JFH1/R167G RNA-transfected cells continued to increase and reached a peak of 2.7×10^5 fmol/liter 54 days after transfection, at which point most cells were core protein positive (Fig. 6B). The core protein level in the medium with MA/N3H+N5BX-JFH1 RNA-transfected cells did not increase and core-positive cells were scarce on day 54 (Fig. 6B). We analyzed the viral genome in the culture supernatants from day 54 for possible mutations and identified four nonsynonymous mutations in the MA/N3H+N5BX-JFH1/R167G genome: L814S (NS2), R1012G, (NS2), T1106A (NS3), and V1951A (NS4B). In order to test whether these amino acid substitutions enhance infectious virus production, L814S, R1012G, T1106A, and V1951A were introduced into MA/N3H+N5BX-JFH1/R167G, and the product was designated MA/N3H+N5BX-JFH1/5am (where am indicates adaptive mutation). On day 1, although HCV core protein levels in the MA/N3H+N5BX-JFH1/5am RNA-transfected cells were higher than those of MA/N3H+N5BX-JFH1/R167G RNA-transfected cells, they were still lower than those of MA/JFH-1.2/R167G RNA-transfected cells; however, on days 3 and 5, they reached a level comparable to that of MA/JFH-1.2/R167G RNA-transfected cells (Fig. 6C). HCV core protein and HCV RNA levels in the medium of MA/N3H+N5BX-JFH1/5am RNA-transfected cells were higher than those of MA/JFH-1.2/R167G RNA-transfected cells ($P < 0.05$, Fig. 6D and 6E, respectively). MA/N3H+N5BX-JFH1/5am, containing the four additional adaptive mutations, produced infectious virus at the same level as MA/JFH-1.2/R167G on day 5 (Fig. 6F). These results indicate that the

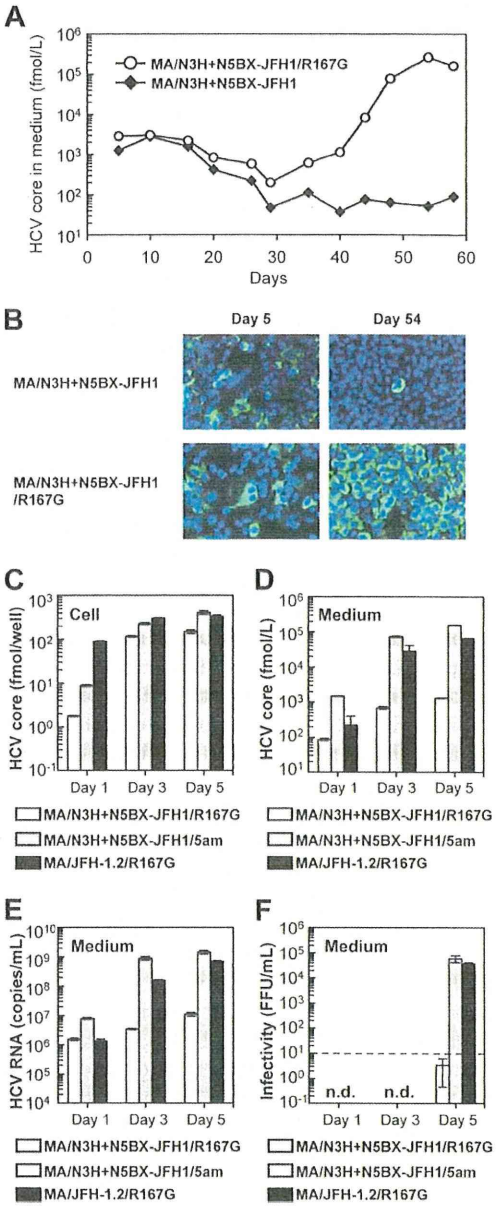

FIG 6 Cell culture-adaptive mutations enhanced infectious virus production of MA/N3H+N5BX-JFH1/R167G. (A) Long-term culture of MA/N3H+N5BX-JFH1 and MA/N3H+N5BX-JFH1/R167G RNA-transfected cells. Ten micrograms of HCV RNA was transfected into Huh7.5.1 cells, and cells were passaged every 2 to 5 days, depending on cell status. Culture medium was collected after every passage, and HCV core protein levels were measured. HCV core protein levels in culture medium from MA/N3H+N5BX-JFH1 and MA/N3H+N5BX-JFH1/R167G RNA-transfected cells are presented. (B) Immunostained cells on days 5 and 54 after transfection. Infected cells were visualized with anti-core antibody (green), and nuclei were visualized with DAPI (blue). (C to F) Effect of four additional cell culture-adaptive mutations on virus production. Ten micrograms of HCV RNA was transfected into Huh7.5.1 cells, and cells and medium were harvested on days 1, 3, and 5. HCV core levels in cells (C) and in medium (D) and HCV RNA levels in medium (E) were measured, and infectivity of medium (F) was determined. Assays were performed three times independently, and data are presented as means ± standard deviation. n.d., not determined. Dashed line indicates the detection limit.

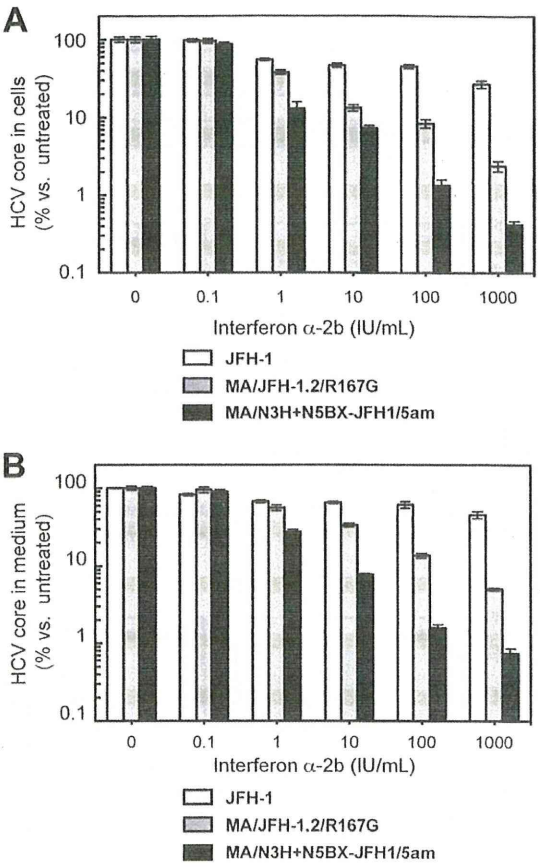

FIG 7 Comparisons of interferon sensitivity between JFH-1, MA/JFH-1.2/R167G and MA/N3H+N5BX-JFH1/5am. Two micrograms of HCV RNA was transfected into Huh7.5.1 cells, and interferon was added at the indicated concentrations at 4 h after transfection. HCV core protein levels in cells (A) and in medium (B) on day 3 were measured, and data are expressed as percent versus untreated cells (0 IU/ml). Assays were performed three times independently, and data are presented as means ± standard deviation.

four additional adaptive mutations enhance infectious virus production and that MA/N3H+N5BX-JFH1/5am RNA-transfected cells replicate and produce infectious virus as efficiently as MA/JFH-1.2/R167G RNA-transfected cells.

Comparison of interferon sensitivity between JFH-1, MA/JFH-1.2/R167G, and MA/N3H+N5BX-JFH1/R167G. Using the newly established genotype 2b infectious chimeric virus, we compared interferon sensitivity between the JFH-1, MA/JFH-1.2/R167G, and MA/N3H+N5BX-JFH1/5am viruses. JFH-1 or MA chimeric viral RNA-transfected Huh7.5.1 cells were treated with 0.1, 1, 10, 100, or 1,000 IU/ml interferon α-2b, and HCV core protein levels in the cells and in culture media were compared. Interferon decreased HCV core protein levels in the JFH-1 RNA-transfected cells and in the medium in a dose-dependent manner, and production was inhibited to 26.8% ± 3.0% and 45.6% ± 4.7%, respectively, of control levels (Fig. 7A and B, respectively). In contrast, HCV core protein levels in cells and medium of MA/JFH-1.2/R167G and MA/N3H+N5BX-JFH1/5am RNA-transfected cells decreased more pronouncedly in a dose-dependent manner (Fig. 7A and B, respectively). HCV core protein levels in cells and medium from MA/N3H+N5BX-JFH1/5am RNA-transfected cells were lower than those from MA/JFH-1.2/